Chemical Geology 378–379 (2014) 24–39

Contents lists available at ScienceDirect

Chemical Geology

journal homepage: www.elsevier.com/locate/chemgeo

Geochemistry of the Abulangdang intrusion: Cumulates of high-Ti picritic magmas in the Emeishan large igneous province, SW China

Christina Yan Wang [a,*], Mei-Fu Zhou [b], Shenghong Yang [c], Liang Qi [d], Yali Sun [e]

[a] Key Laboratory of Mineralogy and Metallogeny, Guangzhou Institute of Geochemistry, Chinese Academy of Sciences, Guangzhou 510640, China
[b] Department of Earth Sciences, The University of Hong Kong, Hong Kong, China
[c] University of Oulu, Oulu, Finland
[d] State Key Laboratory of Ore Deposit Geochemistry, Institute of Geochemistry, Chinese Academy of Sciences, Guiyang 550002, China
[e] State Key Laboratory of Isotopic Geochemistry, Guangzhou Institute of Geochemistry, Chinese Academy of Sciences, Guangzhou 510640, China

ARTICLE INFO

Article history:
Received 10 August 2013
Received in revised form 1 April 2014
Accepted 2 April 2014
Available online 18 April 2014

Editor: L. Reisberg

Keywords:
High-Ti picritic cumulates
The Abulangdang intrusion
Platinum-group elements
Re–Os isotopes
Emeishan large igneous province (SW China)

ABSTRACT

The ~260 Ma Abulangdang ultramafic intrusion in the Panxi region, SW China, is part of the Emeishan large igneous province (ELIP). The intrusion is composed of dunite and lherzolite with minor olivine gabbro. Olivine crystals in the dunite have Fo values from 89.0 to 86.5 mol%. Chromite grains in both the dunite and lherzolite contain more than 0.5 wt.% TiO_2 and show a trend of increasing Fe^{3+} with increasing $Fe^{2+}/(Mg + Fe^{2+})$. Rocks of the intrusion have $\gamma Os(t)$ values from +0.1 to +1.2 and $\varepsilon Nd(t)$ values from −1.9 to +2.9, similar to the high-Ti picrites, high-Ti flood basalts and Fe–Ti oxide-bearing, gabbroic intrusions of the ELIP. Modeling indicates that the Abulangdang intrusion formed by accumulation of olivine and chromite from a high-Ti picritic magma, whereas the high-Ti flood basalts and Fe–Ti oxide-bearing, gabbroic intrusions formed from derivative, evolved magmas after the early fractionation of minerals from the high-Ti picritic magma. Both the dunite and lherzolite have relatively high PGE concentrations and primitive mantle-normalized chalcophile element patterns with positive Os and Ru anomalies, in contrast to PGE-poor high-Ti flood basalts with negative Os and Ru anomalies. This is consistent with the retention of Ru–Os–Ir trace phases with olivine and chromite in the formation of the Abulangdang intrusion. Using a clinopyroxene geobarometer, the crystallization pressure of the Abulangdang intrusion is calculated to be 7.1 to 8.3 kbar, equivalent to a depth of ~21 to 24 km, which is deeper than that estimated for the Fe–Ti oxide-bearing, gabbroic layered intrusions of the ELIP (~5 kbar). We propose that large volumes of mantle plume-derived high-Ti picritic magma underplating along the Moho boundary underwent early fractionation before eruption, and some high-Ti picritic magma ascended through a fossil conduit where the Abulangdang intrusion formed. Residual, evolved magmas either from the conduits or underplating magma chamber formed Fe–Ti oxide-bearing, gabbroic layered intrusions or high-Ti flood basalts. In this fashion, the Abulangdang intrusion resembles ultramafic portions that are missing in the Fe–Ti oxide-bearing, gabbroic intrusions of the ELIP.

1. Introduction

Mantle-derived magmas may have already undergone fractionation of minerals, particularly olivine and chromite, before they are erupted from volcanoes or emplaced into magma chambers (Wilson, 1989). In the Emeishan large igneous province (ELIP), the most abundant volcanic rocks are either evolved low-Ti or high-Ti flood basalts (Zhang et al., 1988; Xu et al., 2001; Xiao et al., 2004; Wang et al., 2007). There are only sparse picrites in the ELIP volcanic succession, which are thought to represent parental magma (*e.g.*, Chung and Jahn, 1995; Zhang et al., 2006; Wang et al., 2007; Hanski et al., 2010). Most of the parental magma may have been trapped at the crust–mantle boundary because of the density contrast (Zhu et al., 2003), a view supported by seismic tomographic modeling which reveals a ~20-km-thick lower crust with P-wave velocities of 7.1–7.8 km/s beneath the ELIP (Yuan, 1989; Liu et al., 2001). The high-velocity lower crust beneath the ELIP was thought to be composed of cumulates formed by cooling and fractionation of melts at the crust–mantle boundary due to high melt production in the plume center (Xu et al., 2004). Picrites of the ELIP provide evidence that minor amounts of parental magma did pass through the crust before undergoing extensive fractionation. On the other hand, extensive studies have demonstrated that gabbroic layered intrusions that host Fe–Ti oxide deposits in the ELIP were derived from evolved magmas (*i.e.*, Zhou et al., 2005; Shellnutt et al., 2009; Zhong et al., 2011). It is thus important to identify intrusions that formed by accumulation of early crystallized minerals from picritic magma in order to test proposed models for the evolution of the ELIP

* Corresponding author.
E-mail address: wang_yan@gig.ac.cn (C.Y. Wang).

http://dx.doi.org/10.1016/j.chemgeo.2014.04.010
0009-2541/

parental magma. Early crystallization of chromite at depth may have led to the formation of economically important chromite deposits in the ELIP. Thus, cumulates of picritic magma may be significant targets for exploration of stratiform chromite deposits in the ELIP.

The Abulangdang intrusion in the Panxi region is the first example of a cumulate body derived from picritic magma in the ELIP. The intrusion is mainly composed of dunite and lherzolite with minor olivine gabbro. Olivine crystals in the dunite and lherzolite have Fo values ranging from 89 to 83 mol%, indicating a magnesian parental magma. It is thus important to determine if there is a genetic link between the ultramafic cumulates represented by the Abulangdang intrusion and the picrites, flood basalts and Fe–Ti oxide-bearing, gabbroic layered intrusions of the ELIP.

Chalcophile elements, Ni, Cu and platinum-group elements (PGE), can be used to investigate the processes involved in the generation of mafic magmas (Barnes et al., 1985; Keays, 1995; Crocket, 2002; Crocket and Paul, 2008). Re–Os isotopic systematics can be used to examine the nature of mantle sources (Walker et al., 1994; Shirey and Walker, 1998; Walker et al., 1999). Thus, both lithophile and chalcophile elements and Re–Os and Sm–Nd isotopes are powerful tools for investigating mantle sources and fractional crystallization of mafic magmas (Barnes et al., 1985; Walker et al., 1994; Crocket and Paul, 2008).

In this paper, we present new major and trace element and PGE data and Re–Os and Sr–Nd isotopic values for the rocks of the Abulangdang intrusion. Using this new dataset, we identify the composition of the parental magma and investigate the role of early fractional crystallization in the formation of the Abulangdang intrusion. We also discuss the possible genetic relationship of the Abulangdang intrusion with the picrites, high-Ti flood basalts and Fe–Ti oxide-bearing, gabbroic layered intrusions of the ELIP. This study has broad implications for understanding the magmatic processes related to the formation of major Fe–Ti oxide-bearing, gabbroic layered intrusions of the ELIP and elsewhere.

2. Geological background

In SW China, the Yangtze Block is bounded by the Tibetan Plateau to the west, and the Indochina Block to the south. The Yangtze Block has a Mesoproterozoic basement overlain by Neoproterozoic to Cenozoic cover (Yan et al., 2003). Rocks of the ELIP in the western Yangtze Block cover an area from SW China to northern Vietnam (inset in Fig. 1). The volcanic succession of the ELIP varies in thickness from several hundred meters to ~5 km and is mainly composed of low-Ti and high-Ti flood basalts, with minor picrite, tephrite and basaltic andesite (Xu et al., 2001; Xiao et al., 2004; Qi et al., 2008). There are also numerous coeval mafic–ultramafic intrusions and granitic and syenitic plutons (Zhou et al., 2008; Shellnutt and Iizuka, 2012). The ELIP is believed to have been formed from a mantle plume at ~260 Ma (Chung and Jahn, 1995).

In the Panzhihua-Xichang (Panxi) district, the flood basalts of the ELIP crop out over a wide area (Fig. 1). Several N–S-trending faults have exposed associated mafic–ultramafic intrusions and granitic and syenitic plutons of the ELIP. The ore-bearing mafic–ultramafic intrusions constitute a mineralized belt about 300 km long and 10 to 30 km wide, forming the most important metallogenic district for Fe, Ti and V in China (Ma et al., 2003; Zhou et al., 2005). The Limahe, Zhubu and Nantianwan intrusions have Ni–Cu–(PGE) sulfide mineralization, whereas the Panzhihua, Baima, Taihe and Hongge layered intrusions host world-class Fe–Ti oxide deposits (Fig. 1). The Fe–Ti oxide-bearing, layered intrusions in the Panxi region are hosted in the Sinian Dengying Formation composed of limestone, but the Xinjie and Hongge bodies locally intruded the Emeishan flood basalts (Zhou et al., 2002a; Zhong et al., 2003). Sulfide-bearing, mafic–ultramafic intrusions are mostly sills in Devonian and Carboniferous strata.

The Abulangdang ultramafic intrusion lies to the west of the major N–S striking Anninghe fault, between Dacao village to the north and Abulangdang village to the south (Fig. 2), and it is hosted in Neoproterozoic gneisses and Sinian strata. The Neoproterozoic gneisses in this region are collectively termed the Kangding Complex, and are composed of granitic gneisses and migmatitic granites (Zhou et al., 2002b), unconformably overlain by Sinian strata.

The ultramafic body was intruded along the axis of the Abulangdang anticline, which plunges south at ~30°. This fold contains the early Sinian dacite in the core and the rocks of the late Sinian Lieguliu and Guanyinya Formation on the limbs (Fig. 2). The limbs of the anticline are crosscut by two N–S striking faults, which control the shape of the intrusion (Fig. 2). The western fault dips 50–85° southeast, whereas the eastern fault dips 45–60° northwest. The intrusion is therefore a N–S striking elongate lopolith, about 8.5 km long and 900 m wide, exposed over an area of ~7.6 km^2 (*e.g.*, Ma et al., 2009). Several E–W striking faults divide the intrusion into segments (Fig. 2).

The Abulangdang intrusion is a concentric body composed of an inner core of coarse-grained dunite (75 vol.%) surrounded by plagioclase-bearing lherzolite (15 vol.%) and olivine gabbro (10 vol.%) (Fig. 2). The various rock types all have transitional boundaries. Zircon grains from the lherzolite yielded a weighted mean $^{206}Pb/^{238}U$ age of 262 ± 2 Ma using the SHRIMP zircon U–Pb technique (Electronic Supplementary material 1), similar to the ages of the mafic–ultramafic intrusions elsewhere in the ELIP (*i.e.*, Zhou et al., 2002a, 2005; Zhong and Zhu, 2006; Zhou et al., 2008; Wang et al., 2012).

3. Petrography

Dunites of the Abulangdang intrusion consist of 85 to 95 modal% olivine, accompanied by 3 to 10% orthopyroxene, <5% clinopyroxene and <2% chromite. The rocks are coarse-grained (0.2 to 2 mm) and exhibit well-developed granoblastic textures with 120° grain boundary intersections, indicating annealing after cooling (Fig. 3a). Smoothly curved boundaries between coarse-grained olivine crystals are common. Clinopyroxene and orthopyroxene are locally interstitial to olivine, whereas chromite occurs as inclusions in the olivine (Fig. 3a).

Lherzolites are composed of 50–85% olivine, 5–10% clinopyroxene, 5–15% orthopyroxene, 5–15% plagioclase and minor chromite (<3%) and sulfide (<2%) (Fig. 3b). Euhedral to subhedral olivine crystals vary in size from 0.2 to 4 mm, and they are enclosed in large clinopyroxene grains to form a poikilitic texture (Fig. 3b). Plagioclase occupies angular interstices between olivine grains to form an intergranular texture (Fig. 3c). Clinopyroxene has augite compositions of $En_{52–56}Wo_{37–42}Fs_{4–8}$, whereas orthopyroxene has enstatite compositions of $En_{84–88}Fs_{9–14}Wo_{0–2}$. Both pyroxenes occur as anhedral crystals 3–6 mm in diameter. Plagioclase has labradoritic compositions ($An_{47–70}$), and typically occurs as coarse-grained, tabular crystals 1 to 2 mm wide. Granular or elongated chromite grains (40–250 μm) are either enclosed in olivine or interstitial to pyroxene and plagioclase crystals (Fig. 3d). Sulfide is interstitial and is closely associated with chromite (Fig. 3e). Platinum-group minerals (PGM) are rare and tiny, the recognized PGM in the dunites is laurite $Ru(Os, Ir)S_2$, one euhedral grain is ~10 μm and is associated with chromite, the other tiny one is ~1 μm in size. Both chromite and laurite are enclosed in olivine (Fig. 3f).

Rocks of the Abulangdang intrusion may have experienced weakly hydrothermal alteration. The rocks are generally fresh although some olivine grains are altered to serpentine along fractures, or to iddingsite or talc on their margins.

4. Analytical results

Dunite and lherzolite samples were collected from two exposed profiles of the Abulangdang intrusion in the Dacao and Abulangdang village, respectively. The locality of the section in the Abulangdang village is 26°52′39″N and 101°48′12″E, whereas the one in the Dacao village is 26°56′6.1″N and 101°48′1.3″E. Sample locations are shown in Fig. 2. Samples were collected for mineral compositions and whole-rock major and trace element analyses including PGE, and Sr–Nd and

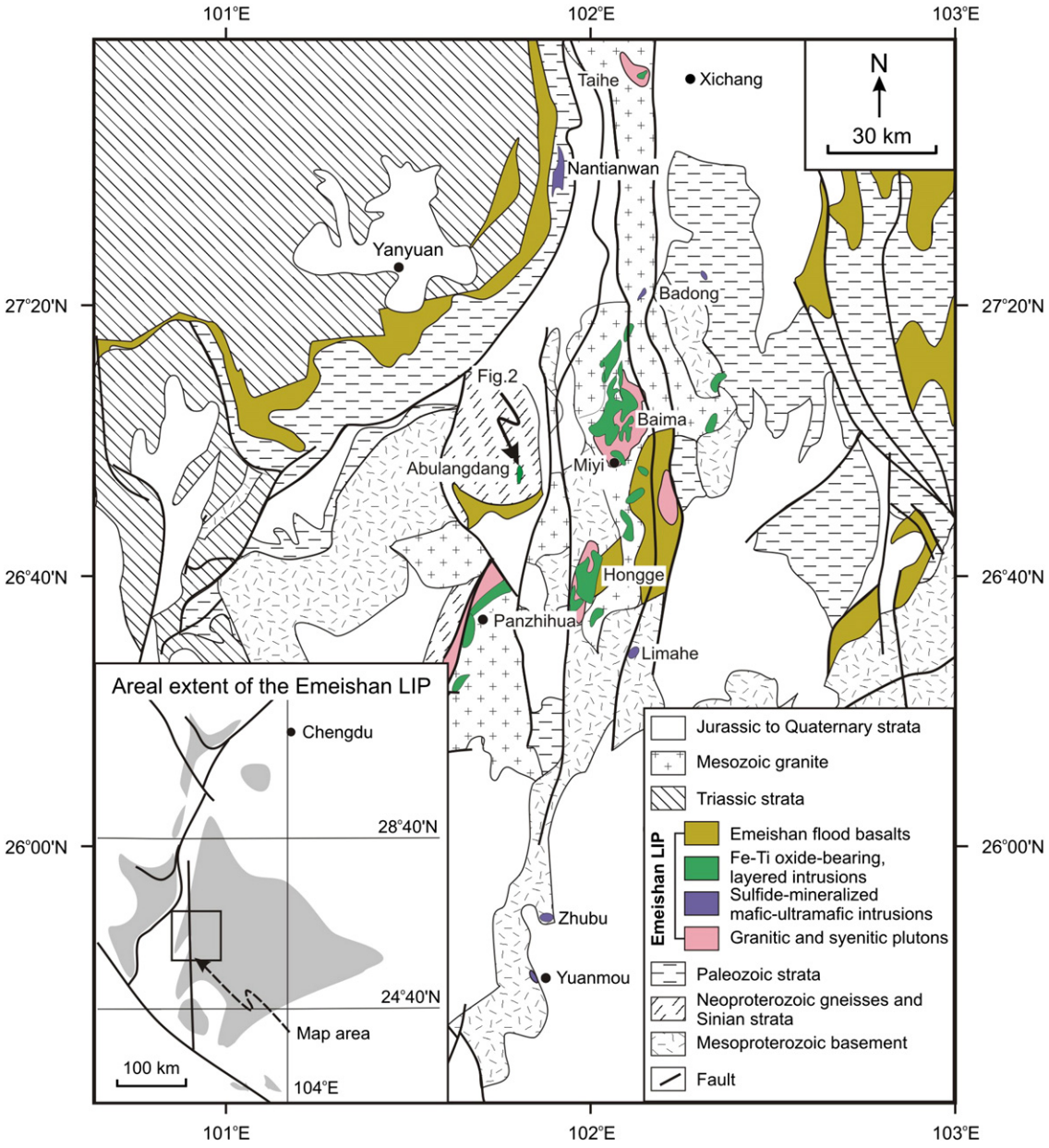

Fig. 1. A simplified geological map of the Pan-Xi area, Emeishan large igneous province, SW China, showing the location of the Abulangdang intrusion and the distribution of layered mafic–ultramafic intrusions and the Emeishan flood basalts in the Panxi region (after Pang et al., 2009).

Re–Os isotopes. Detailed analytical methods are available in the Electronic Supplementary materials 2, 3 and 4.

4.1. Mineral chemistry

Olivine grains in the dunites have Fo contents of 89.0 to 86.5 mol% and NiO of 0.30 to 0.43 wt.%, whereas those in the lherzolites have slightly lower Fo contents of 88.2 to 83.0 mol% and NiO of 0.20 to 0.40 wt.% (Table 1 in Electronic Supplementary material 2). The NiO contents of the olivine grains in the dunites are similar to those of the olivine grains in the picrites of ELIP at similar Fo contents (Fig. 4a), however, there is no significant correlation between Fo and NiO contents of the olivine grains in the Abulangdang intrusion (Fig. 4a). Olivine grains in both the dunites and lherzolites have very low CaO contents (0.03 to 0.16 wt.%), much lower than the olivine grains (CaO = 0.25 to 0.51 wt.%) in the picrites of the ELIP (Li et al., 2012) at the same Fo values (89 to 83) (Fig. 4b).

Chromite grains in the lherzolites have more variable compositions than those in the dunites (Table 2 in Electronic Supplementary material 2). They have variable TiO_2 from 0.7 to 5.2 wt.% (Fig. 5a), and show a positive correlation between $Fe^{3+}/(Fe^{3+}+Al+Cr)$ and $Fe^{2+}/(Mg+Fe^{2+})$, which is defined as a Fe–Ti trend by Barnes and Roeder (2001) (Fig. 5b).

4.2. Whole-rock major and trace elements

Samples of the Abulangdang intrusion have low sulfide contents and low loss-on-ignition (LOI) (<2.8 wt.%), with the exception of two samples with relatively high LOI values (>4 wt.%) (Table 3 in Electronic Supplementary material 3). The whole-rock analyses are normalized to a volatile-free basis. The dunites have 41.6 to 45.1 wt.% MgO, substantially higher than the lherzolites (Fig. 6). The lherzolites contain 0.33 to 0.86 wt.% TiO_2 (Fig. 6b), somewhat higher than the dunites, whereas their FeO_{total} contents (10.0 to 13.2 wt.%) are lower (Fig. 6f). The most

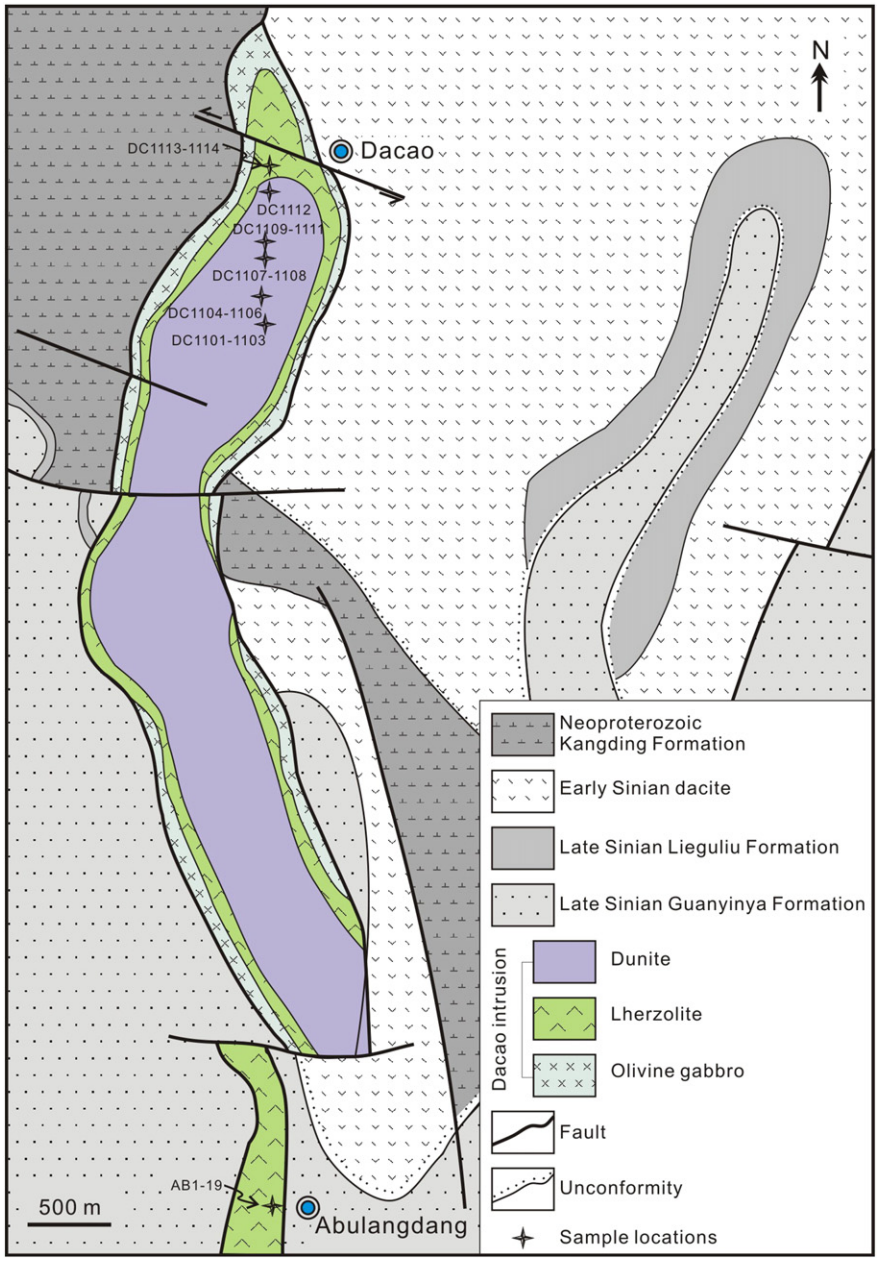

Fig. 2. A geological map of the Abulangdang intrusion showing that the intrusion is a concentric body with an inner core of dunite surrounded by lherzolite which in turn, is rimmed by olivine gabbro (after Wang, 1990; Ge, 2001).

magnesian dunites have whole-rock compositions identical to the average composition of olivine of the intrusion (Fig. 6).

All samples have low REE concentrations, but the dunites have REE even lower than the lherzolites (Fig. 7a). Both the dunites and lherzolites have chondrite-normalized REE patterns with slight LREE-enrichment (Fig. 7a) and $(La/Yb)_N$ from 1.9 to 7.2 and 3.0 to 7.1, respectively. In the primitive mantle-normalized trace element patterns, the dunites show positive Sr and Ti anomalies, whereas the lherzolites show slightly negative Nb anomalies (Fig. 7b).

Both the dunites and lherzolites have similar primitive mantle-normalized chalcophile element patterns, with positive Os and Ru anomalies and either positive or negative Pt and Pd anomalies relative to neighboring elements (Fig. 8 and Table 1). They have chalcophile element patterns comparable with those of the picrites of the ELIP, especially the high-Ti picrites (Fig. 8). Platinum and Pd concentrations are similar to, but Os, Ir and Ru are much higher than those of the high-Ti flood basalts of the ELIP (Fig. 8).

4.3. Whole-rock Sr–Nd and Re–Os isotopes

The dunites from the Abulangdang intrusion have 9.53 to 38.3 ppm Sr and 0.28 to 1.48 ppm Nd, and they have initial $^{87}Sr/^{86}Sr$ ranging from 0.7051 to 0.7057 and $\varepsilon Nd(t = 260\ Ma)$ values from −1.9 to +2.4. The lherzolites have 60.8 to 149 ppm Sr and 3.29 to 9.80 ppm Nd, and they have similar ranges of initial $^{87}Sr/^{86}Sr$ (0.7046 to 0.7060) and $\varepsilon Nd(t)$ values (0 to +2.9) (Table 2 and Fig. 9).

The dunites contain 0.05 to 0.40 ppb Re and 7.5 to 32.0 ppb Os, and have Re/Os of <0.02, whereas the lherzolites have relatively high Re (0.45 to 0.67 ppb) and lower Os (10.1 to 17.3 ppb) (Table 3), yielding higher Re/Os from 0.03 to 0.06. Both the dunites and lherzolites have

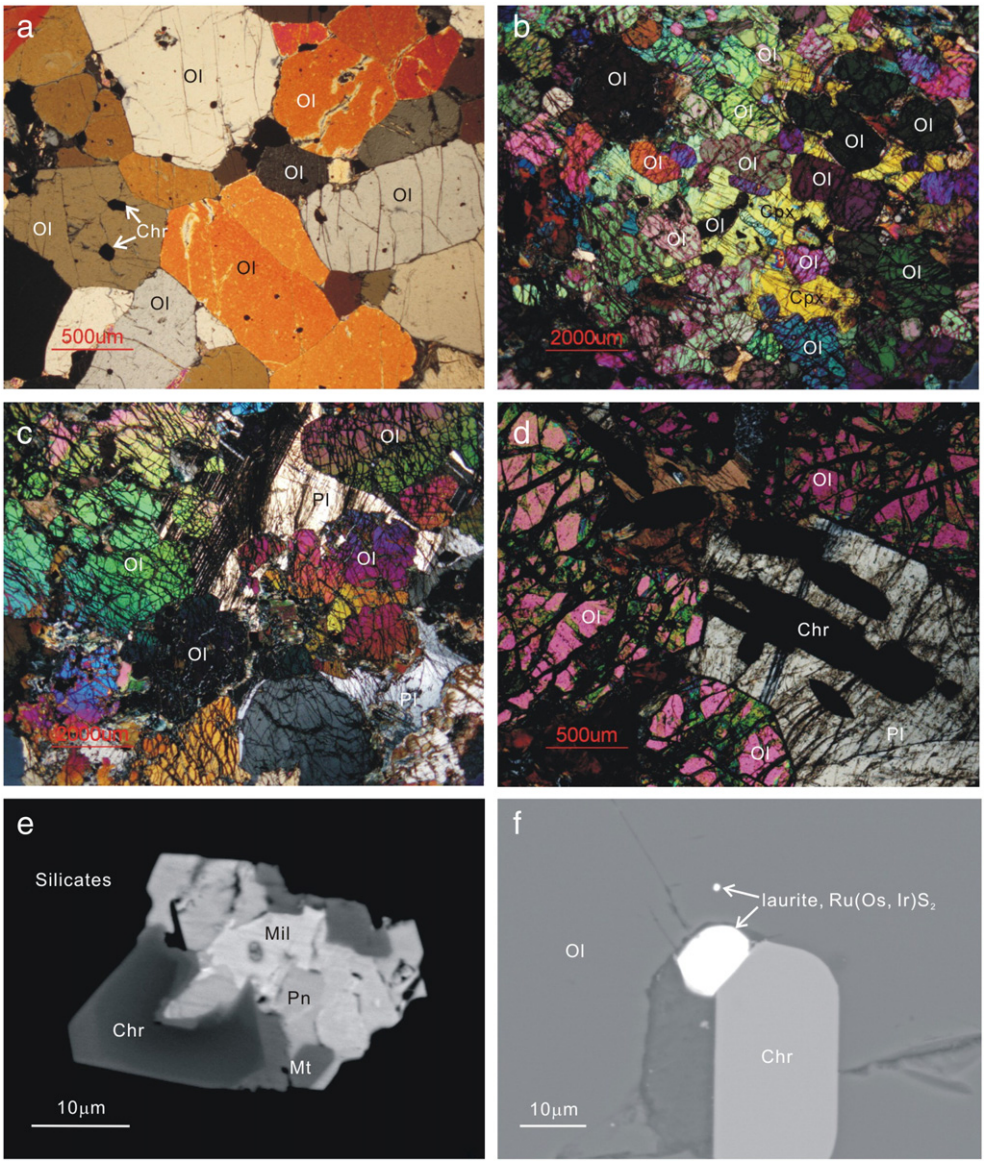

Fig. 3. Photomicrographs of rocks in the dunites and lherzolites of the Abulangdang intrusion. (a) Fine-grained euhedral chromite (Chr) is enclosed within olivine (Ol) in the dunite. Cross polars and transmitted light. Sample DC-1108; (b) a poikilitic texture showing that cumulus olivine grains are enclosed in coarse-grained clinopyroxene (Cpx) in the lherzolite. Cross polars and transmitted light. Sample AB-2; (c) plagioclase (Pl) occupies the angular interstices between olivine grains to form an intergranular texture. Cross polars and transmitted light. Sample AB-12; (d) elongated chromite grains are enclosed in interstitial plagioclase crystals. Cross polars and transmitted light. Sample AB-15; (e) intergrowth of chromite, pantlandite (Pn) and Millerite (Mil) in the interstitial phase, and chromite is surrounded with a thin magnetite (Mt) rim. BSE image. Sample DC1107; (f) laurite is associated with chromite and enclosed in olivine. BSE image. Sample DC1112.

Re/Os much lower than the primitive mantle Re/Os ratios of 0.402 (after Shirey and Walker, 1998), but both have constantly positive, low $\gamma Os(t = 260\ Ma)$ values, with the dunites having $\gamma Os(t)$ values ranging from +0.3 to +1.2, slightly higher than those of the lherzolites (+0.1 to +0.6) (Table 3 and Fig. 10a). The analyses do not generate a good isochron due to the very small range of Re/Os. However, all the samples plot close to a reference isochron of 260 Ma with a $\gamma Os(t)$ value of ~0.5 (Fig. 10b). On the plot of $\gamma Os(t)$ *versus* $\varepsilon Nd(t)$ values (Fig. 11), both the dunites and lherzolites have $\gamma Os(t)$ and $\varepsilon Nd(t)$ values that plot near the field proposed by Shirey and Walker (1998) for the plume mantle. Their $\gamma Os(t)$ values are similar to those of the high-Ti and low-Ti picrites of the ELIP, and much lower than those of the evolved high-Ti flood basalts of the ELIP (Fig. 11). On the other hand, their $\varepsilon Nd(t)$ values are similar to those of the high-Ti picrites and evolved high-Ti flood basalts, but much lower than those of the low-Ti picrites (Fig. 11). They also have $\gamma Os(t)$ and $\varepsilon Nd(t)$ values partially overlapping with the field for the Noril'sk intrusion in the Siberian Traps (Fig. 11).

5. Discussion

5.1. Cumulate origin of the Abulangdang ultramafic intrusion

Olivine grains in both the dunites and lherzolites of the Abulangdang intrusion have 0.03 to 0.16 wt.% CaO (Table 1 in Electronic Supplementary material 2). Olivine in mantle peridotites is generally poor in CaO (<0.1 wt.%, after Simkin and Smith, 1970). High-Fo, low-Ca and high-Ni olivine grains are commonly interpreted as mantle xenocrysts that were picked up from the mantle through which the magma ascended (Ramsay et al., 1984; Cameron, 1985; Boudier, 1991; Hirano et al., 2004; Schuth et al., 2004; Rohrbach et al., 2005), rather than cumulus olivine crystals that crystallized from magmas. However, several lines of

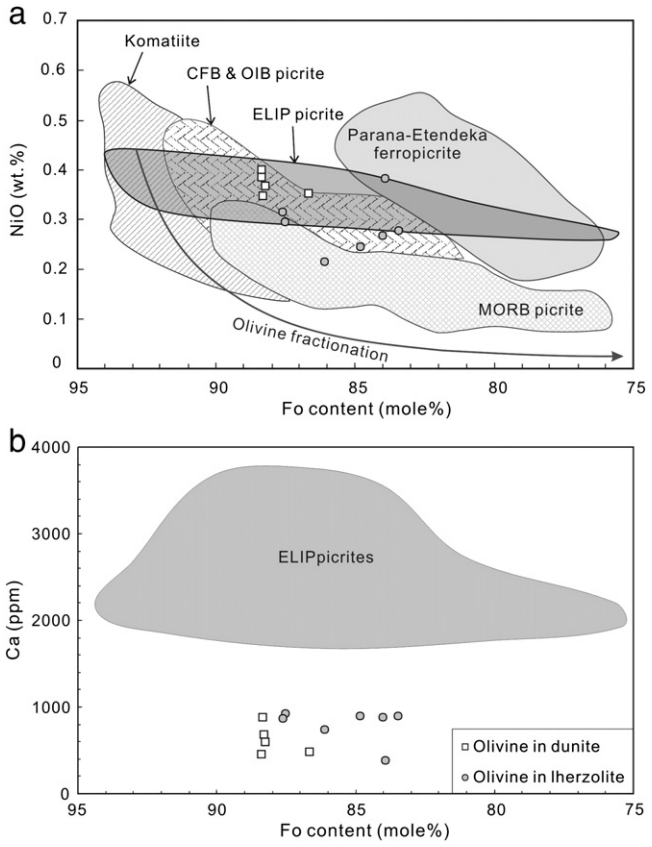

Fig. 4. Plots of Fo *versus* NiO (a) and Fo *versus* Ca (b) for olivine crystals of the Abulangdang intrusion. Note that the each point is the average value of all analyzed points in one thin section. Reference areas in (a) for komatiite, CFB and OIB picrites, MORB picrites and Parana-Etendeka ferropicrites are from Tuff et al. (2005), and the olivine fractionation trend in (a) that is defined by the bulk-rock and olivine compositions of a Barberton komatiite is after Tuff et al. (2005); Reference area in (b) for the picrites of the Emeishan large igneous province is from Li et al. (2012).

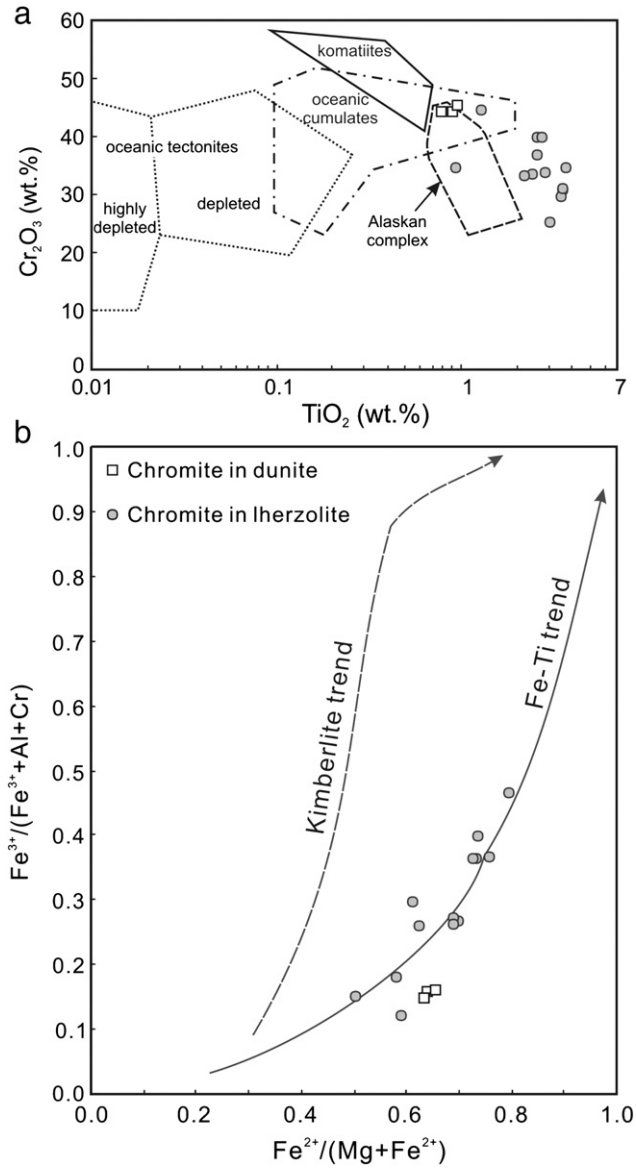

Fig. 5. Plot of TiO_2 *versus* Cr_2O_3 (a) and $Fe^{2+}/(Mg + Fe^{2+})$ *versus* $Fe^{3+}/(Fe^{3+} + Al + Cr)$ of chromite of the Abulangdang intrusion. Note that the each point is an average value for all the analyzed points in one thin section. Chromite composition of different ultramafic rocks in (a) after Herbert (1982); Jan and Windley (1990) and Zhou and Kerrich (1992); kimberlite and the Fe–Ti trend in (b) after Barnes and Roeder (2001).

evidence indicate that Ca-poor olivine grains in the Abulangdang intrusion are cumulus phases rather than mantle xenocrysts. Olivine grains in both the dunites and lherzolites are euhedral to subhedral and show no evidence of deformation such as kink banding (Fig. 3a and b), ruling out a mantle origin. Variable Fo values (89 to 83) of olivine crystals in the dunite and lherzolites are also suggestive of crystallization from magmas, because olivine of mantle xenocrysts is commonly less variable in composition (Kamenetsky et al., 2006). Very high PGE concentrations of the rocks of the Abulangdang intrusion provide additional evidence for a cumulate origin as such high PGE values are not found in mantle peridotite (*i.e.*, Pearson et al., 2004).

Several studies indicate that low-Ca olivine can form from many different types of primitive mantle-derived magmas, such as carbonatite, kimberlite and low-Ca boninite varieties (*e.g.*, Crawford, 1980; Walker and Cameron, 1983; Fedortchouk and Canil, 2004; Kamenetsky et al., 2006). Low-Ca olivine grains are in fact common in the mafic–ultramafic intrusions of the ELIP, such as those in the Ni–Cu–(PGE) sulfide-bearing Jinbaoshan, Limahe and Nantianwan intrusions and the Fe–Ti oxide-bearing Panzhihua and Hongge intrusions (Wang et al., 2005; Pang et al., 2008a; Tao et al., 2008; Pang et al., 2009; Wang et al., 2012) and mafic dikes in the Funing region (Wang et al., 2011). Olivine crystals in these mafic–ultramafic intrusions/dikes have <0.21 wt.% CaO (mostly <0.15 wt.%, *i.e.*, ~1050 ppm Ca), whereas the olivine phenocrysts in the picrites of the ELIP commonly have >0.25 wt.% CaO (~1785 ppm Ca) at similar Fo contents (Li et al., 2012) (Fig. 4b). We consider that the low CaO contents of olivine in these intrusions/dikes may reflect a sub-solidus equilibration between early crystallized olivine and interstitial melt on cooling as the interstitial melt may become Ca-poor with the crystallization of clinopyroxene and plagioclase. However, such an equilibration may not affect the olivine phenocrysts in the picrites which cooled rapidly so that olivine grains in the picrites have CaO contents much higher than those in the intrusions and dikes.

The average compositions of olivine grains in both the dunites and lherzolites are similar to the whole-rock compositions of most magnesian dunite samples of the Abulangdang intrusion (Fig. 6), consistent with the suggestion that the magnesian dunites are adcumulates with minor amounts of intercumulus liquid. Therefore, the olivine crystals in the dunites were in equilibrium with the parental magma when they crystallized. In this case, the olivine is assumed to be the only solid phase on the liquidus before the crystal–liquid system became closed, so we can estimate the liquid composition based on olivine–liquid compositional relationships (*after* Li and Ripley, 2011). Using the composition of the most primitive olivine (Fo = 89) in the Abulangdang intrusion, the olivine–liquid Fe–Mg exchange coefficient, or $K_D = 0.3$ (Roeder and Emslie, 1970), and the average composition of the dunites, the major oxide contents of the parental magma

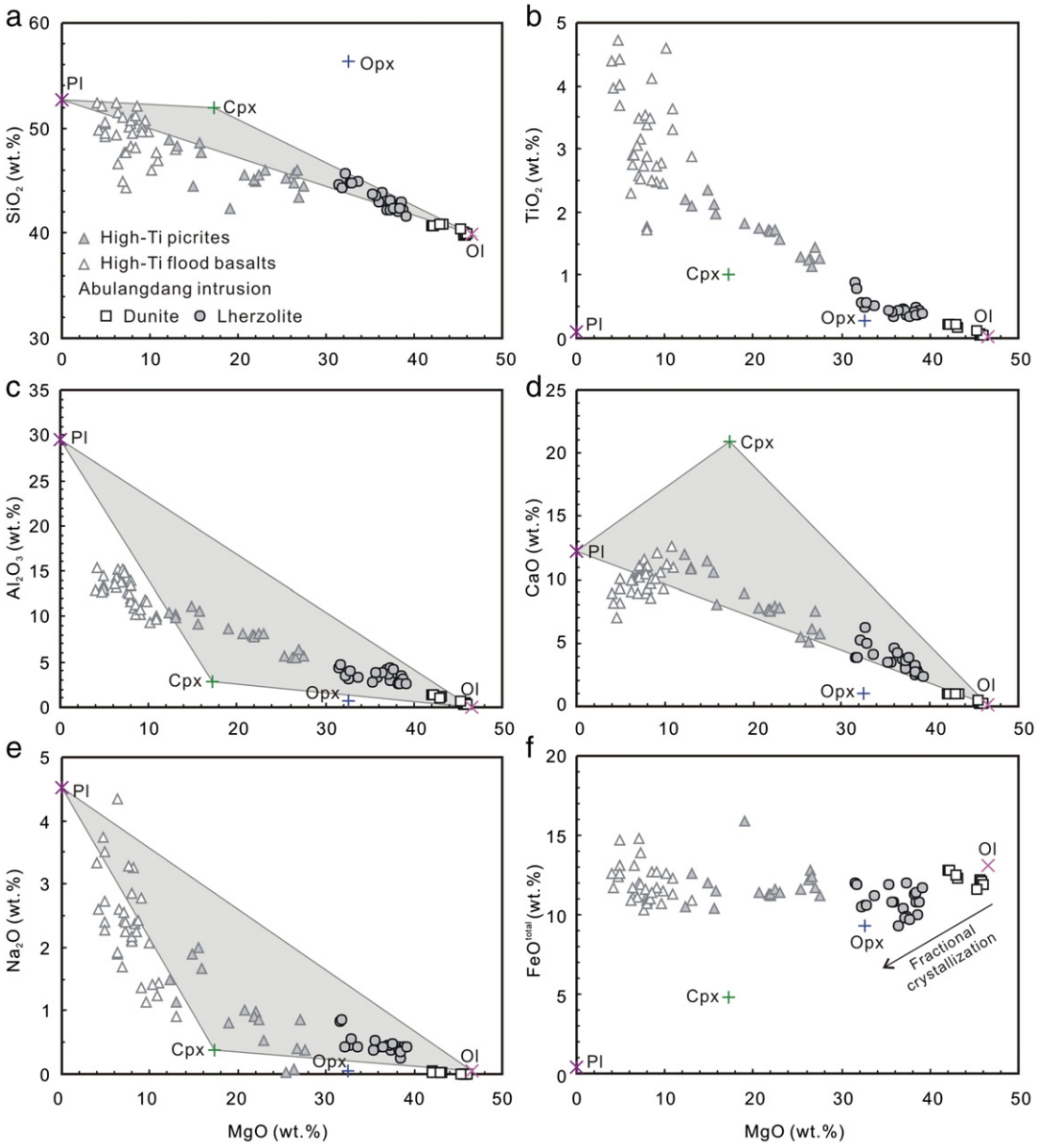

Fig. 6. Variation of SiO_2 (a), TiO_2 (b), Al_2O_3 (c), CaO (d), Na_2O (e) and FeO^{total} (f) against MgO for the rocks of the Abulangdang intrusion. Mineral abbreviations are the same as in Fig. 3, and the mineral composition is the average value for each of the minerals analyzed in this study. Data source: The high-Ti picrites of the ELIP include those in the Dali (Hanski et al., 2010) and Lijiang regions (Zhang et al., 2006); high-Ti flood basalts of the ELIP include those in the Binchuan (Xiao et al., 2004), Miyi and Ertan (Xu et al., 2001) and Longzhoushan regions (Qi et al., 2008).

estimated based on the method of Li and Ripley (2011) are 40.5 wt.% SiO_2, 0.7 wt.% TiO_2, 4.48 wt.% Al_2O_3, 0.91 wt.% MnO, 28.9 wt.% MgO, 19.0 wt.% FeO_t, 2.92 wt.% CaO, 0.07 wt.% Na_2O, 0.13 wt.% K_2O and 0.15 wt.% P_2O_5. The MgO/FeO_t (~1.5) of the parental magma is comparable with that of melt inclusions enclosed in the olivine (Fo = 92) in the high-Ti picrites of the ELIP (Kamenetsky et al., 2012). Therefore, we consider that the Abulangdang intrusion contains cumulus olivines that may have crystallized from the most magnesian parental magma. This may explain why the rocks of the Abulangdang intrusion have much higher MgO than the mafic–ultramafic intrusions elsewhere in the ELIP.

5.2. Crystallization of chromite from a Fe–Ti rich magma

Chromite grains in both the dunites and lherzolites of the Abulangdang intrusion have >0.5 wt.% TiO_2, different from those of oceanic tectonites, komatiites and Alaskan-type complexes (Fig. 5a). Chromite grains in the dunites have a narrow range of TiO_2 from ~0.8 to 1.4 wt.%, whereas those in the lherzolites have a range from 0.8 to 6 wt.%. The range of TiO_2 could be related to extensive, localized reaction with highly fractionated, trapped intercumulus silicate melt (*c.f.*, Barnes and Tang, 1999). It is also possible that the Ti-rich chromite crystallized from a high-Ti parental magma, like that of the Insizwa intrusion in South Africa (Cawthorn et al., 1991). The lack of intimate coexistence of low- and high-Ti chromite on a thin section scale argues for precipitation from high-Ti magma rather than reaction with intercumulus melts (*c.f.*, Barnes and Tang, 1999).

Chromite in mafic–ultramafic intrusions that experienced fractional crystallization of olivine and pyroxene (with or without plagioclase) from a mafic parental magma commonly shows a Fe–Ti trend, a trend of increasing Fe^{3+} with increasing $Fe^{2+}/(Mg + Fe^{2+})$ in the plot of $Fe^{2+}/(Mg + Fe^{2+})$ *versus* $Fe^{3+}/(Fe^{3+}+Cr + Al)$ (Fig. 5b) (Barnes and Roeder, 2001). Increasing $Fe^{2+}/(Mg + Fe^{2+})$ along the Fe–Ti trend can result from exchange of Fe^{2+} and Mg between chromite and

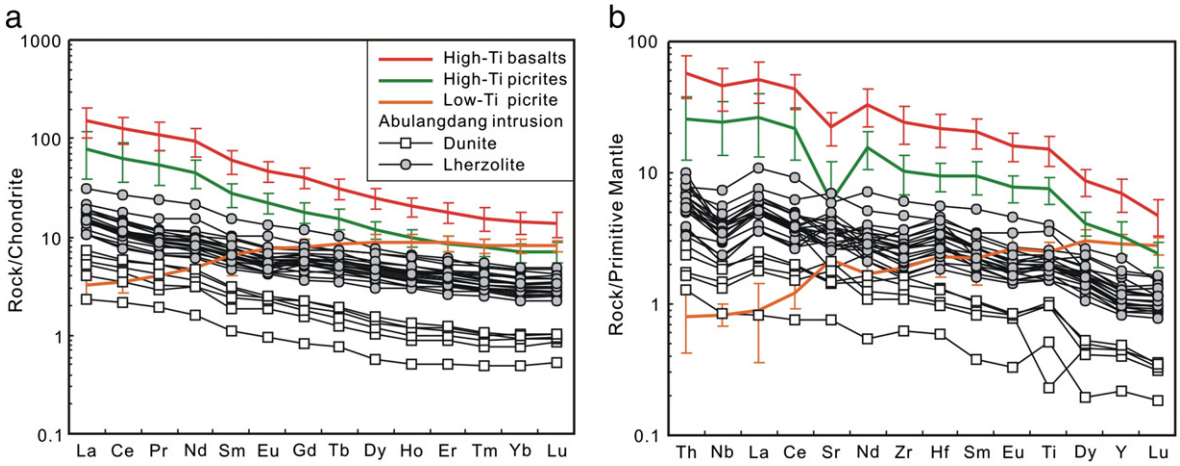

Fig. 7. Chondrite-normalized rare earth element (REE) patterns (a) and primitive mantle-normalized trace element patterns (b) for the rocks of the Abulangdang intrusion. Normalizing values are from Sun and McDonough (1989). The REE and trace element patterns of the high-Ti flood basalts, high-Ti picrites and low-Ti picrites of the ELIP are shown as averaged values for comparison. Data source: high-Ti flood basalts in the Binchuan and Longzhoushan sections after Xiao et al. (2004) and Qi et al.(2008); high-Ti picrites from the Lijiang and Dali regions after Zhang et al. (2006) and Hanski et al. (2010); low-Ti picrite in the Song Da region after Hanski et al. (2004) and Wang et al. (2007).

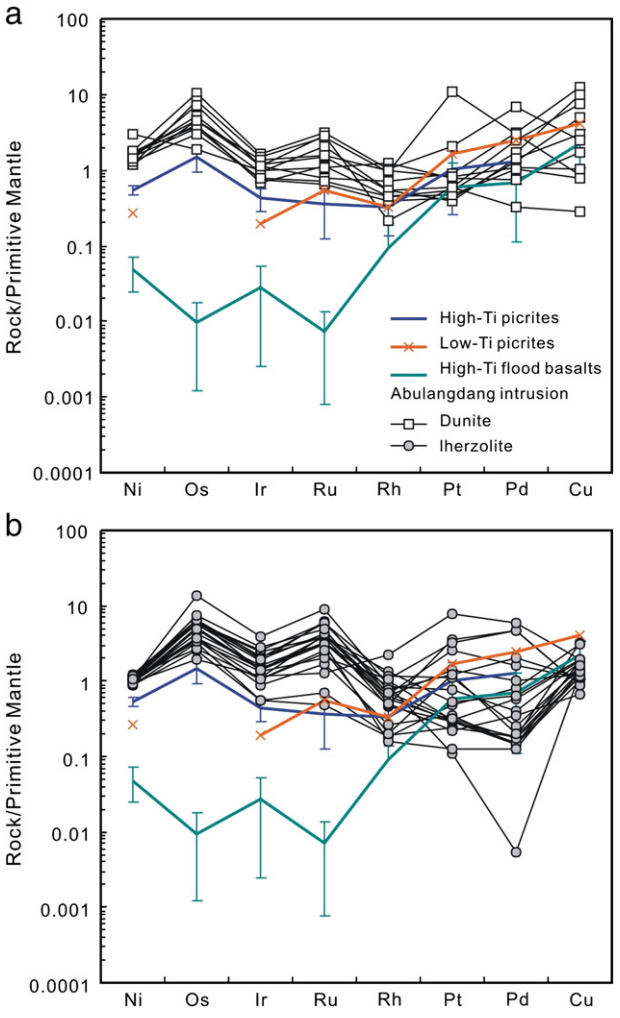

Fig. 8. Primitive mantle-normalized chalcophile element patterns for the rocks of the Abulangdang intrusion. Normalizing values are from Barnes and Maier (1999) and references therein. The patterns of the high-Ti flood basalts, high-Ti picrites and low-Ti picrites of the ELIP are shown as averaged values for comparison. Data sources: high-Ti picrites in Lijiang after Zhang et al. (2006); high-Ti flood basalts in Longzhoushan after Qi et al. (2008); low-Ti picrites in Song Da after Wang et al. (2007).

coexisting olivine on cooling (Irvine, 1965). Chromite grains in the dunites of the Abulangdang intrusion plot near the Fe–Ti trend but with somewhat higher $Fe^{2+}/(Mg + Fe^{2+})$ ratios (Fig. 5b). Given the high Fo values of coexisting olivine in the dunite, the high $Fe^{2+}/(Mg + Fe^{2+})$ ratios of the chromite are likely due to sub-solidus exchange of Fe^{2+} and Mg between chromite and olivine. However, chromite grains in the lherzolites have Cr_2O_3 lower and TiO_2 higher than those in the dunites (Fig. 5a), and plot along the Fe–Ti trend (Fig. 5b). Increasing $Fe^{2+}/(Mg + Fe^{2+})$ ratios of the chromite grains in the lherzolites are interpreted as a result of crystallization from evolved Fe–Ti rich magmas. This indicates that the parental magma may have become more enriched in Fe and Ti with fractionation.

5.3. Fractionation of primitive high-Ti picritic magmas

Picrites and ferrobasalts of the ELIP are considered to represent the parental magma of the flood basalts and related mafic–ultramafic intrusions (Zhou et al., 2005; Zhang et al., 2006; Hanski et al., 2010; Kamenetsky et al., 2012). Hanski et al. (2010) summarized the primitive, high-Mg volcanic rocks of the ELIP and recognized them as LREE-depleted, low-Ti komatiites and picrites, and LREE-enriched, high-Ti picrites. Based on the published data set, picrites in the Jinping and Song Da regions of the southernmost ELIP have $FeO_t < \sim 11$ wt.% and $TiO_2 < 1$ wt.% and LREE-depleted patterns (Hanski et al., 2004; Wang et al., 2007; Anh et al., 2011) and are denoted as LREE-depleted, low-Ti varieties, whereas those in the Dali and Lijiang areas of the central ELIP have $FeO_t > \sim 11$ wt.% and $TiO_2 > 1.5$ wt.% and LREE-enriched patterns (*c.f.*, Chung and Jahn, 1995; Song et al., 2001; Xu et al., 2001; Xiao et al., 2004; Zhang et al., 2006; Hanski et al., 2010; Li et al., 2010), and are referred to LREE-enriched, high-Ti varieties. Melt inclusions enclosed in the olivines of the low-Ti and high-Ti picrites have <10 wt.% and >12 wt.% FeO_t, respectively (Kamenetsky et al., 2012), indicating that they are distinctly different varieties. We denoted them as low-Ti and high-Ti picrites in this study for consistency with the literature.

There are linear trends of major oxides against MgO for the high-Ti picrites, high-Ti flood basalts and the Abulangdang intrusion (Fig. 6). The negative correlations of MgO *versus* Al_2O_3, CaO, and Na_2O are consistent with fractionation of plagioclase, clinopyroxene and orthopyroxene (Fig. 6c, d and e). The high-Ti picrites and flood basalts of the ELIP and the Abulangdang intrusion all have parallel chondrite-normalized REE patterns (Fig. 7a), differing only in the degree of

Table 1
Platinum-group elements and Cu and Ni concentrations for the rocks of the Abulangdang intrusion.

	Ni (ppm)	Cu (ppm)	Os (ppb)	Ir (ppb)	Ir (ppb)	Ru (ppb)	Ru (ppb)	Rh (ppb)	Rh (ppb)	Pt (ppb)	Pt (ppb)	Pd (ppb)	Pd (ppb)
Analytical methods			Fire assay	Fire assay	*Carius tube*	Fire assay	*Carius tube*	Fire assay	*Carius tube*	Fire assay	*Carius tube*	Fire assay	*Carius tube*
Dunite													
DC1101	3110	381	17.3	3.87		3.92		0.67		6.36		12.5	
DC1102	2970	147	12.2	2.51		3.26		0.38		3.05		5.17	
DC1103	3180	296	13.4	2.32		5.60		0.42		3.76		6.84	
DC1104	3290	88.4	15.3	4.00		7.50		0.52		2.75		5.74	
DC1105	3300	226	12.6	3.15		10.2		0.51		4.24		9.82	
DC1106	5770	51.5	6.48	3.32		5.41		1.19		5.52		2.96	
DC1107	3460	75.9	35.3	5.60		15.6		0.97		14.3		27.5	
DC1108	2310	25.7	28.4	5.11		13.4		0.90		76.3		12.0	
DC1109	2370	30.8	15.5	4.58		7.77		0.95		5.74		4.28	
DC1110	2560	21.3											
DC1111	2530	23.2	10.3	2.65		3.62		0.43		3.33		4.11	
DC1112	2800	8.63	24.2	3.93		14.4		0.20		4.21		1.27	
Lherzolite													
DC1113	1700	96.7	10.9	1.87		3.50		0.19		1.68		0.72	
DC1114	1710	94	8.64	1.86		2.39		0.17		3.37		3.18	
AB1	2253	33.7	18.9	6.37	6.97	30.3	25.5	0.63	0.64	18.2	21.6	6.50	8.51
AB2	1996	52.5	14.8	5.42	5.71	15.8	16.6	0.80	0.71	5.39	6.24	1.64	2.18
AB3	1960	56.0	19.9	8.18	9.73	19.5	21.2	0.95	0.97	2.10	2.20	2.33	2.99
AB4	2237	30.1	21.9	4.73		19.7		0.44		2.06		0.58	
AB5	2106	37.6	45.9	12.9		44.0		0.83		0.75		0.02	
AB6	2236	27.1	9.25	3.69	3.61	11.5	11.0	0.46	0.52	24.4	28.5	18.8	24.1
AB7	2215	35.9		3.78		20.3		0.61		9.62		4.10	
AB8	1874	55.2	12.3	3.03		8.46		0.25		2.46		0.57	
AB9	2356	59.4	21.9	7.40	9.38	19.7	19.9	1.27	1.38	3.79	3.86	2.61	3.33
AB10	1994	40.5	12.6	5.02		16.2		0.62		2.00		0.72	
AB11	2167	44.3	20.1	8.85	8.93	29.5	27.5	1.12	0.94	7.97	7.23	1.00	1.60
AB12	1875	35.2	17.1	4.99		16.0		0.55		2.17		0.62	
AB13	2077	26.0	11.6	4.53	5.61	10.0	9.42	1.01	0.89	22.5	21.0	18.6	21.3
AB14	2274	33.6	20.5	6.78	8.02	30.0	26.3	0.72	0.73	8.74	9.78	8.02	10.6
AB15	1974	34.8	22.1	6.76	6.77	21.1	19.4	0.68	0.64	2.27	2.51	0.68	1.46
AB16	1872	58.7	6.50	3.96	4.21	6.31	6.05	2.12	2.12	53.8	56.8	23.9	28.9
AB17	2125	19.7	24.8	9.46	10.49	25.1	22.3	0.49	0.53	1.51	1.64	1.39	2.02
AB18	1780	39.5	16.9	4.80	5.26	15.3	15.0	0.15	0.15	0.87	1.45	0.50	0.55
AB19	2061	47.5	12.4	3.64		12.7		0.19		8.37		0.81	
Standards													
WPR-1(expected)					13.5		22		13.4		285		235
WPR-1 (this study)					11.7		22.0		12.6		305		244
GPt-4 (expected)			2.4	4.7		2.5		4.3		58		60	
GPt-4 (this study)			2.10	4.59		2.25		4.46		48.2		46.5	
GPt-7 (expected)			0.64	1.2		0.66		1.1		14.7		15.2	
GPt-7 (this study)			0.51	1.26		0.36		0.98		13.1		13.4	

Table 2
Rb–Sr and Sm–Nd isotopic compositions for the rocks of the Abulangdang intrusion.

Sample no.	Rb (ppm)	Sr (ppm)	$^{87}Sr/^{86}Sr$	2σ	$^{87}Rb/^{86}Sr$	$(^{87}Sr/^{86}Sr)_i$	Sm (ppm)	Nd (ppm)	$^{143}Nd/^{144}Nd$	2σ	$^{147}Sm/^{144}Nd$	$(^{143}Nd/^{144}Nd)_i$	εNd(t)
Dunite													
DC-1105	0.87	9.53	0.705926	0.000007	0.2577	0.7050	0.05	0.28	0.512604	0.000003	0.1046	0.5124	2.4
DC-1106	2.22	36.9	0.706374	0.000013	0.1698	0.7057	0.28	1.43	0.512416	0.000004	0.1237	0.5122	−1.9
DC-1109	2.11	38.2	0.705960	0.000005	0.1559	0.7054	0.36	1.48	0.512563	0.000003	0.1538	0.5123	0.0
DC-1110	2.20	30.2	0.705987	0.000007	0.2056	0.7052	0.46	2.00	0.512544	0.000002	0.1433	0.5123	−0.1
DC-1111	2.13	30.8	0.705810	0.000003	0.1952	0.7051	0.47	2.21	0.512583	0.000002	0.1340	0.5124	1.0
DC-1112	0.55	16.1	0.706013	0.000009	0.0964	0.7057	0.17	0.74	0.512603	0.000004	0.1442	0.5124	1.1
Lherzolite													
DC-1113	8.08	126	0.705325	0.000005	0.1810	0.7047	2.36	9.80	0.512628	0.000002	0.1518	0.5124	1.3
DC-1114	6.59	149	0.705037	0.000007	0.1248	0.7046	1.56	7.02	0.512541	0.000004	0.1404	0.5123	0.0
AB-1	4.8	95.9	0.705158	0.000011	0.1451	0.7046	1.22	5.32	0.512679	0.000014	0.1387	0.5124	2.7
AB-5	3.50	71.3	0.705333	0.000013	0.1421	0.7048	0.80	3.29	0.512686	0.000012	0.1459	0.5124	2.6
AB-7	4.11	84.4	0.705215	0.000012	0.1410	0.7047	1.11	4.79	0.512675	0.000012	0.1407	0.5124	2.6
AB-9	2.71	67.0	0.705168	0.000013	0.1170	0.7047	1.04	4.19	0.512707	0.000013	0.1498	0.5125	2.9
AB-13	7.21	104	0.706205	0.000012	0.2002	0.7055	1.19	5.32	0.512630	0.000012	0.1357	0.5124	1.9
AB-19	7.02	60.8	0.707235	0.000014	0.3342	0.7060	1.03	4.43	0.512599	0.000013	0.1402	0.5124	1.1

enrichment. The high-Ti flood basalts have the highest REE and the Abulangdang intrusion the lowest (Fig. 7a). As we mentioned earlier, rocks of the Abulangdang intrusion, especially the dunites, are adcumulates with small amounts of trapped liquid, it is therefore the trapped liquid that controls the REE patterns of the rocks because REE are incompatible in olivine ($D < 0.051$, Nielsen et al., 1992), clinopyroxene ($D = 0.0536–0.442$, Hart and Dunn, 1993), orthopyroxene ($D = 0.0008–0.22$, Green et al., 2000) and plagioclase ($D = 0.007–0.271$, Bindeman and Davis, 2000) in basaltic magmas. This explains why the lherzolites have REE enrichment relative to the dunites as the lherzolites contain more clinopyroxene, orthopyroxene and plagioclase that crystallized from the trapped liquid. In this fashion, the linear trends shown in Fig. 6 indicate that the high-Ti flood basalts formed from magma that was more evolved than that of the Abulangdang intrusion. On the other hand, rocks of the Abulangdang intrusion have a range of Sm/Nd similar to those of the high-Ti picrites and flood basalts, and Fe–Ti oxide-bearing, gabbroic layered intrusions of the ELIP (Table 4). These rocks all have LREE-enriched patterns, different from those of the low-Ti picrites of the ELIP (Fig. 7a). The Sm/Nd of the rocks may indicate that they may have derived from a common high-Ti picritic parental magma as the ratio does not change significantly during partial melting or fractional crystallization because both elements are incompatible and have similar partition coefficients in silicate minerals (Rollinson, 1994).

Rocks of the Abulangdang intrusion have primitive mantle-normalized chalcophile element patterns with positive Os and Ru anomalies, whereas the high-Ti flood basalts of the ELIP have negative Os and Ru anomalies (Fig. 8). The high-Ti flood basalts of the ELIP are thought to have been derived from a parental magma formed by low degrees of partial melting of an OIB-like, enriched mantle source (Wang et al., 2007; Zhou et al., 2008), therefore, significant depletion of Os–Ir–Ru in the high-Ti flood basalts is possibly due to the presence of trace phases such as Os–Ir–Ru alloys and PGE sulfides in the mantle

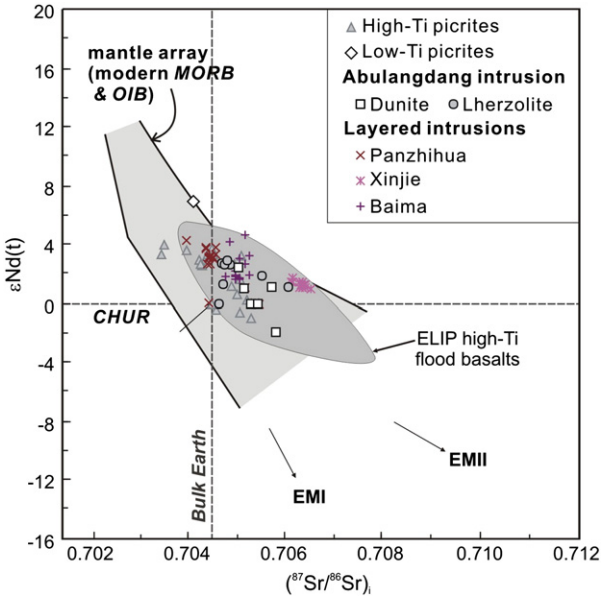

Fig. 9. Plot of εNd(t) (t = 260 Ma) values *versus* initial $^{87}Sr/^{86}Sr$ for the rocks of the Abulangdang intrusion. Data sources: mantle array and modern MORB and OIB range after Ishikawa et al. (2007) and Tappe et al. (2007), EMI and EMII trends after Zindler and Hart (1986); Bulk Earth data from DePaolo (1988); high-Ti flood basalts of the ELIP from Xu et al. (2001), Xiao et al. (2004) and Zhang et al. (2006); high-Ti picrites of the ELIP from Zhang et al. (2006) and Zhang et al. (2008); low-Ti picrites of the ELIP from Wang et al. (2007); Panzhihua intrusion from Zhou et al.(2008) and Zhang et al. (2009); Baima intrusion from Zhou et al. (2008) and Shellnutt et al. (2009); Xinjie intrusion from Zhang et al.(2009).

Table 3
Re–Os isotopic compositions for the rocks of the Abulangdang intrusion.

Sample no.	Re (ppb)	Os (ppb)	$^{187}Re/^{188}Os$	$^{187}Os/^{188}Os$	2σ	$(^{187}Os/^{188}Os)_i$	γOs
Dunite							
DC-1101	0.298	26.6	0.053	0.1260	0.0003	0.1257	0.4
DC-1102	0.178	19.4	0.043	0.1263	0.0007	0.1261	0.6
DC-1103	0.299	23.6	0.060	0.1261	0.0003	0.1259	0.5
DC-1104	0.153	20.7	0.035	0.1262	0.0004	0.1261	0.6
DC-1105	0.238	21.7	0.052	0.1259	0.0004	0.1256	0.3
DC-1106	0.120	8.9	0.064	0.1267	0.0006	0.1264	0.9
DC-1107	0.181	32.0	0.027	0.1258	0.0004	0.1257	0.3
DC-1108	0.398	29.5	0.064	0.1259	0.0006	0.1256	0.3
DC-1109	0.127	12.2	0.049	0.1265	0.0002	0.1263	0.8
DC-1110	0.152	7.6	0.095	0.1265	0.0003	0.1261	0.7
DC-1111	0.151	7.5	0.095	0.1273	0.0002	0.1268	1.2
DC-1112	0.051	28.8	0.008	0.1259	0.0002	0.1259	0.5
Lherzolite							
DC-1113	0.612	9.95	0.291	0.1267	0.0002	0.1254	0.1
DC-1114	0.550	8.91	0.292	0.1269	0.0004	0.1256	0.2
AB-1	0.574	14.6	0.185	0.1262	0.0003	0.1254	0.1
AB-5	0.508	16.3	0.148	0.1267	0.0003	0.1260	0.6
AB-7	0.457	17.3	0.125	0.1261	0.0003	0.1255	0.2
AB-9	0.634	14.7	0.204	0.1268	0.0003	0.1259	0.5
AB-13	0.466	10.8	0.205	0.1265	0.0003	0.1257	0.3
AB-19	0.445	10.1	0.209	0.1265	0.0003	0.1256	0.2

Note: $\gamma Os = 100 \times \left(\frac{(^{187}Os/^{188}Os)_{sample} + (^{187}Re/^{188}Os)_{sample} \times e^{\lambda T} - 1}{(^{187}Os/^{188}Os)i + (^{187}Re/^{188}Os)_{chon} \times \left(e^{\lambda\left(4.558 \times 10^{9}\right)} - e^{\lambda T}\right)} - 1 \right)$,

where $\lambda = 1.666 \times 10^{-11}$ year^{-1}, $T = 260 \times 10^{6}$ year; the primitive initial $^{187}Os/^{188}Os$, $(^{187}Os/^{188}Os)_i$, is assumed to be 0.09531 and the average $^{187}Re/^{188}Os$ of chondrites, $(^{187}Re/^{188}Os)_{chon}$, is 0.40186 (after Shirey and Walker, 1998).

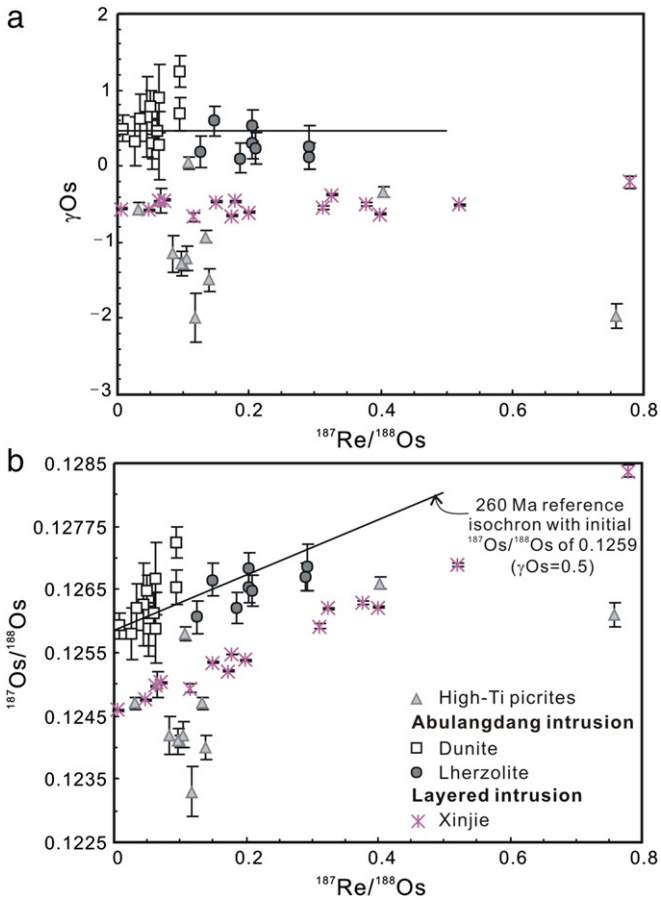

Fig. 10. Plots of $^{187}Re/^{188}Os$ *versus* γOs(t = 260 Ma) values (a) and $^{187}Re/^{188}Os$ *versus* $^{187}Os/^{188}Os$ for the rocks of the Abulangdang intrusion compared with the high-Ti picrites and Xinjie intrusion of the ELIP. Data source: high-Ti picrites after Zhang et al. (2005); Xinjie intrusion after Zhong et al. (2011). The parameters used in the calculation of 260 Ma reference isochron are: $\lambda_{Re} = 1.666 \times 10^{-11}$/year, $(^{187}Re/^{188}Os)_{Chon} = 0.40186$, $(^{187}Os/^{188}Os)_{Chon,0} = 0.1270$ (Shirey and Walker, 1998) and calculated $(^{187}Os/^{188}Os)_{Chon,260\ Ma} = 0.1253$.

(Li et al., 2012). However, the conjugate PGE profiles between the rocks of the Abulangdang intrusion and the high-Ti flood basalts likely reflect the compatibility of IPGE (Os, Ir and Ru) in chromite and trace phases

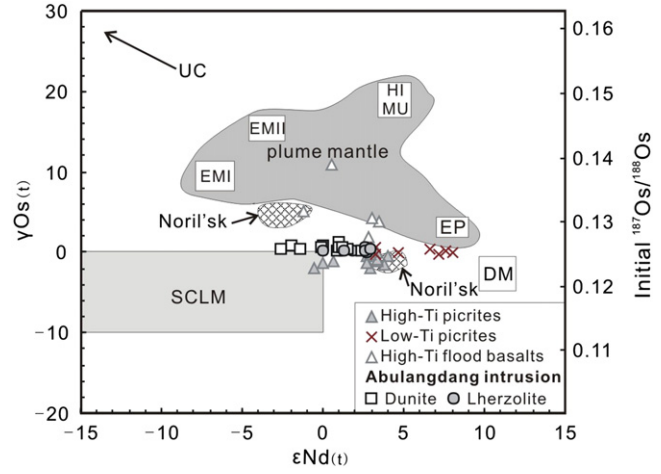

Fig. 11. Plot of γOs(t) and εNd(t) values for the rocks of the Abulangdang intrusion. Data sources: The fields of the reservoir end members of the plume mantle (DM, EP, HIMU, EMI, EMII) and the field of SCLM and the Noril'sk intrusion (251 Ma) are after Shirey and Walker (1998) and references therein; high-Ti flood basalts and high-Ti picrites of the ELIP after Zhang et al. (2008); low-Ti picrite of the ELIP after Hanski et al.(2004).

associated with olivine during fractionation. This is supported by the occurrence of laurite in the olivine of the Abulangdang intrusion (Fig. 3f), and is also evidenced from good correlations of Ir with Os and Ru but poor correlations of Ir with Pt and Pd (Fig. 12). Iridium may also occur as Ir-dominant alloys in ultramafic magmas (Barnes and Fiorentini, 2008), whereas Ru is compatible in chromite (Locmelis et al., 2011). In particular, the partition coefficients of Ru, Rh and Ir in Fe^{3+}-rich chromites are much higher than those for Fe^{3+}-poor spinel (Brenan et al., 2012). The positive correlations of Cr with Os, Ir, and Ru in rocks of the Abulangdang intrusion, as well as high-Ti picrites and flood basalts of the ELIP (Fig. 13) indicate that IPGE may have been incorporated into early crystallized chromite and olivine in the form of laurite and other trace phases. We consider that retention of Os–Ir–Ru trace phases with olivine and chromite of the Abulangdang intrusion may have depleted the remaining melt in these metals. This is consistent with the origin of the high-Ti flood basalts from evolved, high-Ti picritic magmas after separation and accumulation of olivine and chromite.

5.4. An igneous suite derived from the same mantle source

The weakly LREE-enriched, chondrite-normalized REE patterns and negative Nb anomalies in the rocks of the Abulangdang intrusion (Fig. 7a) could be attributed to crustal contamination. The $(Th/Yb)_{PM}$ of whole-rock compositions are considered a sensitive indicator of crustal contamination because Th is only present in mantle-derived rocks at the ppb range as opposed to ppm levels in the crust (McDonough and Sun, 1995), and fractionation of the typical mineral assemblage olivine + orthopyroxene + plagioclase ± chromite in mafic–ultramafic intrusions will not strongly alter the ratio. We thus consider that this proxy can provide a valuable assessment of crustal contamination. The rocks of the Abulangdang intrusion have $(Th/Yb)_{PM}$ ranging from 0.1 to 1.0, much lower than that of the upper continental crust (about 30.5, Weaver and Tarney, 1984). In addition, the rocks of the Abulangdang intrusion have a restricted range of initial $^{87}Sr/^{86}Sr$ (0.705 to 0.706). Therefore, we consider that isotopic compositions and trace elemental patterns of the rocks were not altered by crustal contamination.

All the rocks of the Abulangdang intrusion have εNd(t) values (−1.9 to +2.9) much lower than those of the low-Ti picrites of the ELIP (Fig. 9), which are believed to have been derived from the highly depleted asthenospheric mantle (Hanski et al., 2004; Wang et al., 2007). On the other hand, rocks of the Abulangdang intrusion have εNd(t) values and initial $^{87}Sr/^{86}Sr$ similar to those of the high-Ti picrites and flood basalts and Fe–Ti oxide-bearing, gabbroic layered intrusions of the ELIP (Table 4 and Fig. 9), which are considered to have derived from an OIB-like, enriched mantle source (Wang et al., 2007; Qi et al., 2008; Zhou et al., 2008). In addition, rocks of the Abulangdang intrusion and the high-Ti picrites have similar primitive mantle-normalized chalcophile element patterns from Ni to Rh and they both have relatively high Os, Ir and Ru concentrations compared with those of the high-Ti flood basalts (Fig. 8). The high-Ti picrites of the ELIP have ~2 ppb Os, low Re (0.2 ppb) and low Re/Os (0.02–0.05) and γOs values (−0.4 to −2.0) (Zhang et al., 2008), close to those of the rocks of the Abulangdang intrusion (γOs = +0.1 to +1.2) (Fig. 10). The least contaminated high-Ti basalts in the ELIP have low Re/Os of 0.1 (Xu et al., 2007). The γOs(t) values of the Xinjie Fe–Ti oxide-bearing layered intrusions in the Panxi region range from −0.7 to −0.2 (Zhong et al., 2011), also comparable with the high-Ti flood basalts and high-Ti picrites of the ELIP and the rocks of the Abulangdang intrusion (Table 4). The high-Ti flood basalts and high-Ti picrites have γOs(t) values consistent with the origin deduced from Sr and Nd isotopes of the Abulangdang intrusion and other ELIP samples. We therefore conclude that the Abulangdang intrusion, high-Ti flood basalts, high-Ti picrites and Fe–Ti oxide-bearing, gabbroic layered intrusions of the ELIP comprise an igneous suite derived from the same OIB-like, enriched mantle source.

Table 4
A compiled data set of εNd(t) values, Sm/Nd ratios, initial Sr ratios, γOs(t) values and Re/Os ratios of the Abulangdang intrusion, high-Ti picrites, high-Ti flood basalts and Fe–Ti oxide-bearing, layered intrusions of the Emeishan large igneous province.

	Abulangdang intrusion	High-Ti picrites	High-Ti flood basalts	Mafic–ultramafic layered intrusions
εNd(t)	1.1 to 2.7	Lijiang: −1.0 to 4.0 (Zhang et al., 2006; Zhang et al., 2008)	Binchuan: −1.2 to 0.4 (Xiao et al., 2004) Miyi: −3.6 to 1.1 (Xu et al., 2001) Lijiang: −1.3 to 3.8 (Zhang et al., 2006) Ertan: −2.4 to 4.0 (Xu et al., 2001) Longzhoushan: −4.7 to 2.4 (Xu et al., 2007; Qi et al., 2008)	Panzhihua: −2.1 to 4.3 (Zhou et al., 2008; Zhang et al., 2009) Baima: 1.6 to 4.6 (Zhou et al., 2008; Shellnutt et al., 2009) Hongge: −2.7 to 1.0 (Zhong et al., 2003) Xinjie: 1.0 to 1.4 (Zhong et al., 2011)
Sm/Nd	0.16–0.31	Dali: 0.24–0.26 (Hanski et al., 2010) Lijiang: 0.18–0.23 (Zhang et al., 2006; Hanski et al., 2010)	Binchuan: 0.19–0.25 (Xiao et al., 2004) Miyi: 0.20–0.21 (Xu et al., 2001) Lijiang: 0.19–0.31 (Zhang et al., 2006) Ertan: 0.18–0.24 (Xu et al., 2001) Longzhoushan: 0.18–0.24 (Xu et al., 2007; Qi et al., 2008)	Panzhihua: 0.21–0.33 (Zhou et al., 2008) Baima: 0.20–0.39 (Zhou et al., 2008) Hongge: 0.21–0.32 (Bai et al., 2012) Xinjie: 0.20–0.26 (Zhang et al., 2009)
Initial Sr	0.7046–0.7060	Lijiang: 0.7034–0.7052 (Zhang et al., 2006; Zhang et al., 2008)	Binchuan: 0.7049–0.7064 (Xiao et al., 2004) Miyi: 0.7052–0.7064 (Xu et al., 2001) Lijiang: 0.7038–0.7052 (Zhang et al., 2006) Ertan: 0.7049–0.7063 (Xu et al., 2001) Longzhoushan: 0.7052–0.7086 (Qi et al., 2008)	Panzhihua: 0.7039–0.7053 (Zhou et al., 2008) Baima: 0.7049–0.7052 (Zhou et al., 2008) Hongge:0.7058–0.7064 (Zhong et al., 2003) Xinjie: 0.7061–0.7064 (Zhang et al., 2009)
γOs(t)	0.1 to 1.2	−2.0 to 0 (Zhang et al., 2008)	Longzhoushan (least contaminated): −0.51 (Xu et al., 2007)	Xinjie: −0.7 to 0.6 (Zhong et al., 2011)
Re/Os	0–0.06	0.01–0.03 (Zhang et al., 2008)	Longzhoushan (least contaminated): 0.1 (Xu et al., 2007)	Xinjie: 0–0.11 (Zhong et al., 2011)

5.5. A "missing" ultramafic portion for the Fe–Ti oxide-bearing, gabbroic layered intrusions of the ELIP

Layered intrusions that host Fe–Ti oxide deposits in the Panxi region have olivine crystals with relatively low Fo values (63 to 83 mol%, Zhou, 1982; Wang et al., 2008; Pang et al., 2009; Bai et al., 2012) and ultramafic portions are absent in the Panzhihua, Baima and Taihe intrusions. It is likely that they formed from evolved magmas and that the ultramafic portions of the magmas were left behind during magma ascent. We propose that the Abulangdang intrusion represents the ultramafic portion that was missing in these layered intrusions. If this is the case, cumulates like the Abulangdang intrusion should have formed

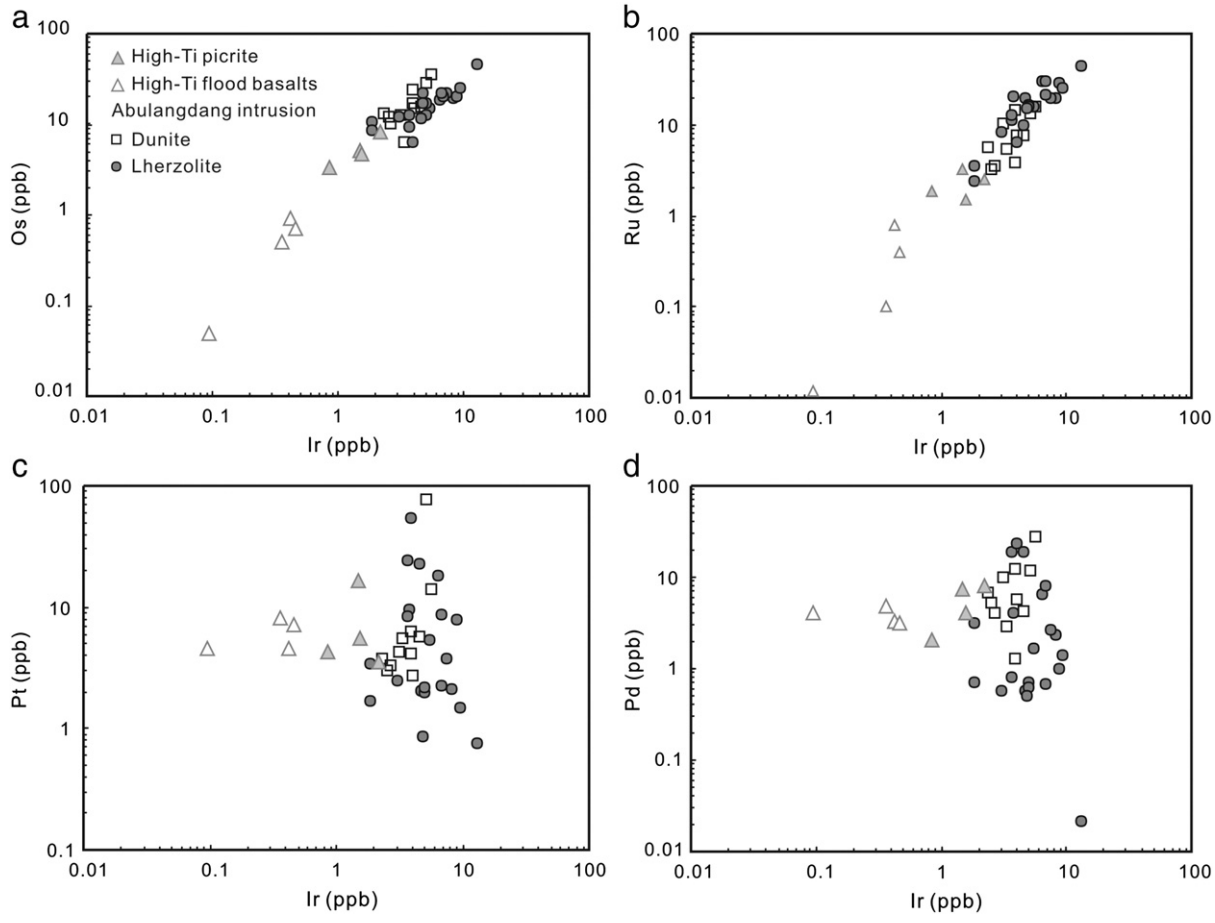

Fig. 12. Plots of Ir *versus* Os, Ru, Pt and Pd for the rocks of the Abulangdang intrusion showing good correlations of Ir and Os, Ru and poor correlations of Ir and Pt, Pd.

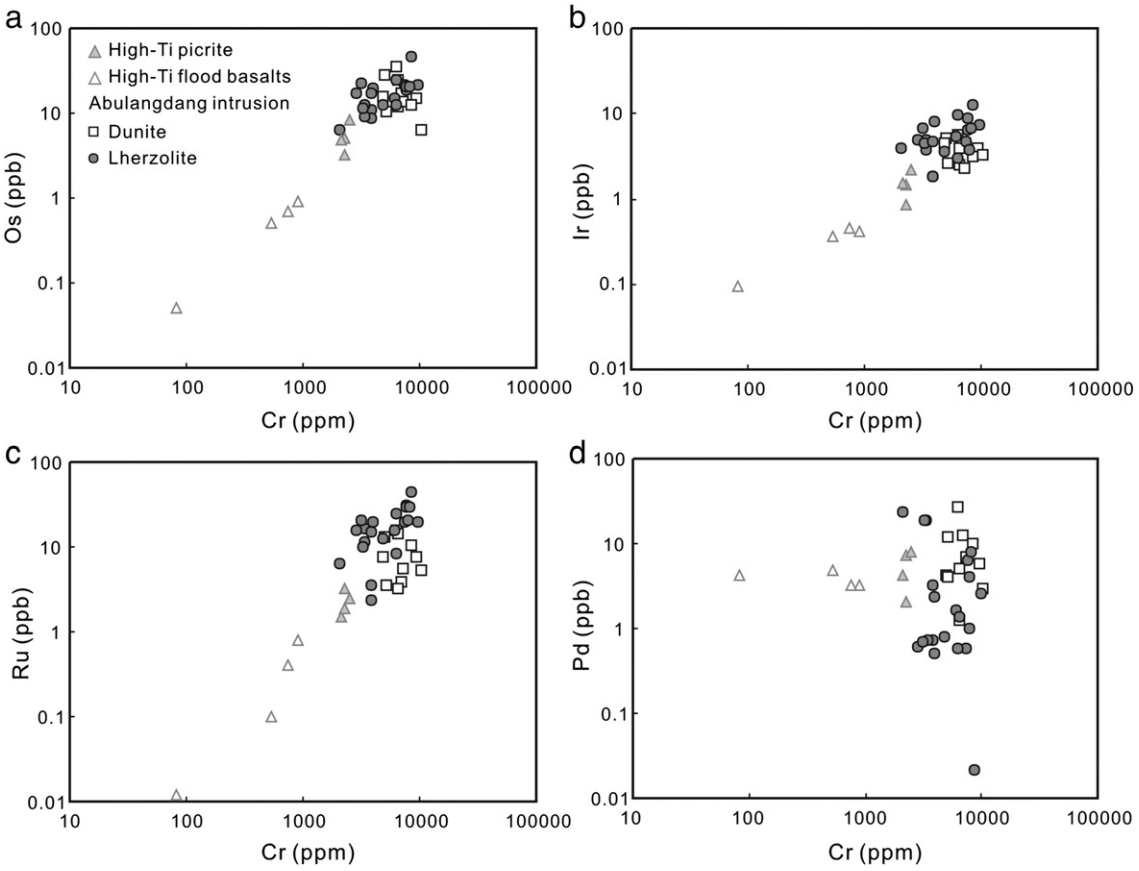

Fig. 13. Plots of Cr *versus* Os, Ir, Ru for the rocks of the Abulangdang intrusion showing good correlations of Cr and Os, Ir, Ru and poor correlation of Cr and Pd.

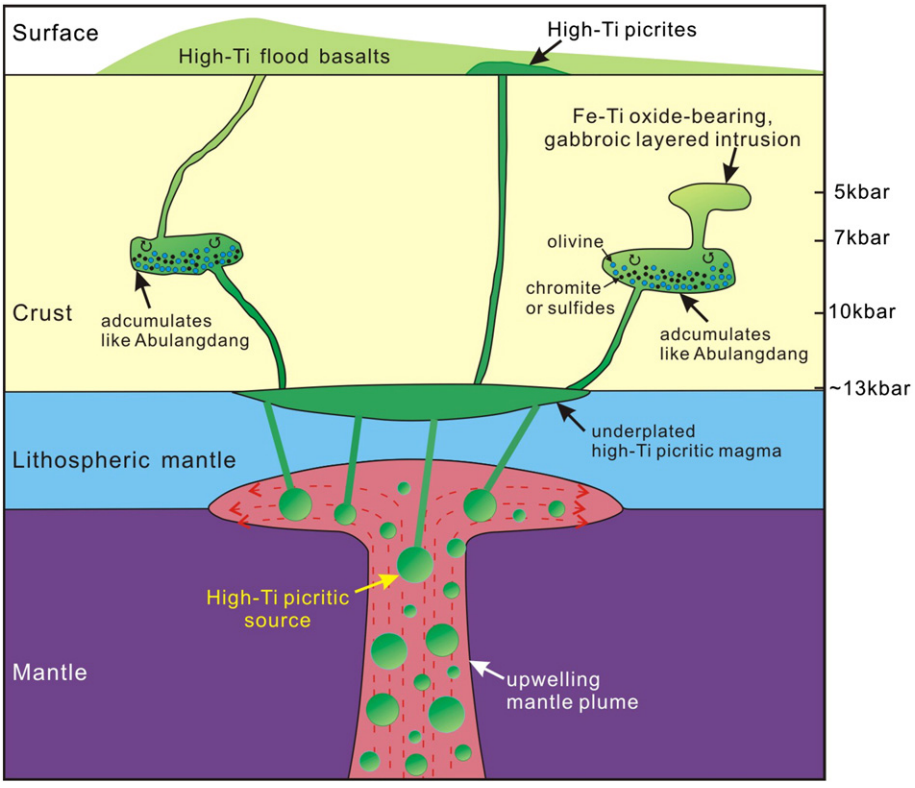

Fig. 14. A schematic cartoon showing extended fractionation processes of the igneous suite of high-Ti picrites, ultramafic cumulates, Fe–Ti oxide-bearing, gabbroic layered intrusions and high-Ti flood basalts of the ELIP.

in deep-seated, staging magma chambers, whereas the layered intrusions formed from evolved magmas that were emplaced into shallower chambers.

To test the possible link between the Fe–Ti oxide-bearing, gabbroic layered intrusions and the Abulangdang intrusion, we calculated the temperature and pressure of emplacement for the Abulangdang intrusion. We used the two-pyroxene thermometer of Brey and Köhler (1990), and clinopyroxene–orthopyroxene pairs from two lherzolite samples, AB5 and AB19, to calculate the equilibration temperature, which varies from 1007 to 1057 °C (Electronic Supplementary material 5). Because the high-Ti picrites and high-Ti flood basalts of the ELIP belong to a mildly alkaline series (Xu et al., 2001), we used clinopyroxene geobarometry for mildly alkaline magma systems to estimate the pressure of crystallization of the rocks (Nimis, 1995, 1999). The pressures are calculated to be 7.1 and 8.3 kbar at 1007 and 1057 °C, respectively, roughly equivalent to a depth of 21 to 24 km. In the previous studies, the Fe–Ti-V-rich ferrobasaltic magma composition of the Panzhihua intrusion suggested by Zhou et al. (2005) has been produced experimentally by crystallizing an olivine tholeiite at ~9.3 kbar under ~0.4 wt.% H_2O (Whitaker et al., 2007). Pang et al. (2008b) thus inferred that the parental magmas of the Panzhihua intrusion may have formed by differentiation of mantle-derived, ferropicritic melts under a pressure of ~10 kbar, probably at the base of the crust, and that the residual magma was then emplaced at a shallower depth (~5 kbar) where it crystallized to produce the Panzhihua intrusion. Our estimate of the pressure of emplacement of the Abulangdang intrusion is comparable with the pressure (~10 kbar) estimated by Pang et al. (2008b) for the formation of the parental magma of the Panzhihua intrusion. A fractionation process using the average composition of the high-Ti picrites of the ELIP at 8 kbar under the QFM buffer was simulated by the MELTS program (Ghiorso and Sack, 1995). The results show that the resultant melt has FeO_t and TiO_2 contents comparable with that of the high-Ti flood basalts at 0.4 wt.% H_2O (Electronic Supplementary material 6). Therefore, we suggest that the large volumes of high-Ti picritic magma that underplated along the Moho boundary in South China ascended and started to fractionate in magma conduits at depths equivalent to ~7 to 10 kbar where an olivine-laden crystal mush formed by crystallization of olivine and chromite in a staging magma chamber. The Abulangdang intrusion is thus one of many such staging magma chambers that may have developed at the same time. The evolved, residual magmas ascended along conduits and were emplaced at shallower levels where they underwent continued fractionation to form layered intrusions, such as Panzhihua, or were erupted to form high-Ti flood basalts (Fig. 14). In this scenario, chromite was likely retained in the staging magma chamber, and the evolved magmas became more Fe- and Ti rich with the fractionation. As a result, Cr-rich titanomagnetite rather than chromite may have become the earliest crystallizing phase from the evolved magmas at shallower magma chambers where the layered intrusions formed, as evidenced from the Cr-rich titanomagnetite in the base of the Xinjie and Hongge layered intrusions of the ELIP (Wang et al., 2008; Bai et al., 2012; Wang and Zhou, 2013). This model can explain how high-Ti flood basalts formed from evolved magmas and why chromite is absent in the mafic–ultramafic layered intrusions of the ELIP.

6. Conclusions

The Abulangdang intrusion represents cumulates from a primitive, high-Ti picritic magma of the ELIP. This intrusion provides strong evidence for the missing link between high-Ti picritic magma and evolved Fe–Ti rich magmas that were emplaced to form Fe–Ti oxide-bearing, gabbroic layered intrusions or erupted to form high-Ti flood basalts of the ELIP. The association of cumulates like the Abulangdang intrusion, with high-Ti flood basalts, Fe–Ti oxide-bearing, gabbroic layered intrusions and high-Ti picrites of the ELIP, provides a good example of such an extended fractionation process.

Supplementary data to this article can be found online at http://dx.doi.org/10.1016/j.chemgeo.2014.04.010.

Acknowledgment

Financial support for this study was provided by a Chinese National "973" project (2011CB808903) to CYW, a grant from the Research Grant Council of Hong Kong (HKU707012P) to MFZ and NSFC Grant Nos. 41121002 and 41325006. We thank Jianqi Wang at Northwest University for his assistance with analyses of major elements of dunite samples, and Jianfeng Gao at the University of Hong Kong for the analyses of Sr and Nd isotopes. We appreciate a big help from Peter Fisher and Hazel Prichard at Cardiff University in characterizing the platinum-group minerals in the thin sections. Constructive comments from two reviewers, Paul Robinson and K.N. Pang, and editor Laurie Reisberg, are essential to improve the manuscript. This is contribution No. IS-1865 from GIGCAS.

References

Anh, T.V., Pang, K.-N., Chung, S.-L., Lin, H.-M., Hoa, T.T., Anh, T.T., Yang, H.-J., 2011. The Song Da magmatic suite revisited: a petrologic, geochemical and Sr–Nd isotopic study on picrites, flood basalts and silicic volcanic rocks. J. Asian Earth Sci. 42, 1341–1355.
Bai, Z.J., Zhong, H., Naldrett, A.J., Zhu, W.G., Xu, G.W., 2012. Whole-rock and mineral composition constraints on the genesis of the giant Hongge Fe–Ti–V oxide deposit in the Emeishan large igneous province, southwest China. Econ. Geol. 107, 507–524.
Barnes, S.J., Fiorentini, M.L., 2008. Iridium, ruthenium and rhodium in komatiites: evidence for iridium alloy saturation. Chem. Geol. 257, 44–58.
Barnes, S.-J., Maier, W.D., 1999. The fractionation of Ni, Cu and the noble metals in silicate and sulfide liquids. In: Keays, R.R., Lesher, C.M., Lightfoot, P.C., Farrow, C.E.G. (Eds.), Dynamic processes in magmatic ore deposits and their application to mineral exploration. Geological Association of Canada, Short Course Notes, 13, pp. 69–106.
Barnes, S.J., Roeder, P.L., 2001. The range of spinel compositions in terrestrial mafic and ultramafic rocks. J. Petrol. 42, 2279–2302.
Barnes, S.J., Tang, Z.L., 1999. Chrome spinels from the Jinchuan Ni–Cu sulphide deposit, Gansu Province, People's Republic of China. Econ. Geol. 94, 343–356.
Barnes, S.-J., Naldrett, A.J., Gorton, M.P., 1985. The origin of the fractionation of platinum-group elements in terrestrial magmas. Chem. Geol. 53, 303–323.
Bindeman, I., Davis, A., 2000. Trace element partitioning between plagioclase and melt: investigation of dopant influence on partition behavior. Geochim. Cosmochim. Acta 64, 2863–2878.
Boudier, F., 1991. Olivine xenocrysts in picritic magmas: an experimental and microstructural study. Contrib. Mineral. Petrol. 109, 114–123.
Brenan, J.M., Finnigan, C.F., McDonough, W.F., Homolova, V., 2012. Experimental constraints on the partitioning of Ru, Rh, Ir, Pt and Pd between chromite and silicate melt: the importance of ferric iron. Chem. Geol. 302–303, 16–32.
Brey, G.P., Köhler, T., 1990. Geothermobarometry in four-phase lherzolites II. New thermobarometers, and practical assessment of existing thermobarometers. J. Petrol. 31, 1353–1378.
Cameron, W.E., 1985. Petrology and origin of primitive lavas from the Troodos ophiolite, Cyprus. Contrib. Mineral. Petrol. 89, 239–255.
Cawthorn, R.G., de Wit, M., Hatton, C.J., Cassidy, K.F., 1991. Ti-rich chromian spinel from the Mount Ayliff intrusion, Transkei: further evidence for high Ti tholeiitic magma. Am. Mineral. 76, 562–573.
Chung, S.-L., Jahn, B.-M., 1995. Plume–lithosphere interaction in generation of the Emeishan flood basalts at the Permian–Triassic boundary. Geology 23, 889–892.
Crawford, A.J., 1980. A clinoenstatite-bearing cumulate olivine pyroxenite from Howqua, Victoria. Contrib. Mineral. Petrol. 75, 353–367.
Crocket, J.H., 2002. Platinum-group element geochemistry of mafic and ultramafic rocks. In: Cabri, L.J. (Ed.), Geology, geochemistry, mineralogy and mineral beneficiation of platinum-group elements. Canadian Institute of Mineralogy Metallogeny Petrology, Special volume, 54, pp. 177–210.
Crocket, J.H., Paul, D.K., 2008. Platinum-group elements in igneous rocks of the Kutch rift basin, NW India: implications for relationships with the Deccan volcanic province. Chem. Geol. 248, 239–255.
Depaolo, D.J., 1988. Neodymium Isotope Geochemistry: an Introduction. Springer Verlag, New York.
Fedortchouk, Y., Canil, D., 2004. Intensive variables in kimberlite magmas, Lac de Gras, Canada and implications for diamond survival. J. Petrol. 45, 1725–1745.
Ge, M.X., 2001. Geological features and prospecting perspective for the Dacao Cu–Ni–Pt deposit in Miyi. J. Sichuan Geol. 21, 223–225 (In Chinese).
Ghiorso, M.S., Sack, R.O., 1995. Chemical mass transfer in magmatic processes IV. A revised and internally consistent thermodynamic model for the interpolation and extrapolation of liquid–solid equilibria in magmatic systems at elevated temperatures and pressures. Contrib. Mineral. Petrol. 119, 197–212.
Green, T., Blundy, J., Adam, J., Yaxley, G., 2000. SIMS determination of trace element partition coefficients between garnet, clinopyroxene and hydrous basaltic liquids at 2–7.5 GPa and 1080–1200 C. Lithos 53, 165–187.

Hanski, E., Walker, R.J., Huhma, H., Polyakov, G.V., Balykin, P.A., Hoa, T.T., Phuong, N.T., 2004. Origin of the Permian–Triassic komatiites, northwestern Vietnam. Contrib. Mineral. Petrol. 147, 453–469.
Hanski, E., Kamenetsky, V.S., Luo, Z.Y., Xu, Y.G., Kuzmin, D.V., 2010. Primitive magmas in the Emeishan Large Igneous Province, southwestern China and northern Vietnam. Lithos 119, 75–90.
Hart, S.R., Dunn, T., 1993. Experimental cpx/melt partitioning of 24 trace elements. Contrib. Mineral. Petrol. 113, 1–8.
Herbert, R., 1982. Petrography and mineralogy of oceanic peridotites and gabbros: some comparisons with ophiolite examples. Ofioliti 7, 299–324.
Hirano, N., Yamamoto, J., Kagi, H., Ishii, T., 2004. Young, olivine xenocryst-bearing alkali-basalt from the oceanward slope of the Japan Trench. Contrib. Mineral. Petrol. 148, 47–54.
Irvine, T.N., 1965. Chromian spinel as a petrogenetic indicator. Part 1. Theory. Can. J. Earth Sci. 2, 648–672.
Ishikawa, A., Kuritani, T., Makishima, A., Nakamura, Eizo, 2007. Ancient recycled crust beneath the Ontong Java Plateau: isotopic evidence from the garnet clinopyroxenite xenoliths, Malaita, Solomon Islands. Earth Planet. Sci. Lett. 259, 134–148.
Jan, M.Q., Windley, B.F., 1990. Chromian spinel-silicate chemistry in ultramafic rocks of the Jijal complex, northwest Pakistan. J. Petrol. 31, 667–715.
Kamenetsky, V.S., Elburg, M., Arculus, R., Thomas, R., 2006. Magmatic origin of low-Ca olivine in subduction-related magmas: co-existence of contrasting magmas. Chem. Geol. 233, 346–357.
Kamenetsky, V.S., Chung, S.-L., Kamenetsky, M.B., Kuzmin, D.V., 2012. Picrites from the emeishan large igneous province, SW China: a compositional continuum in primitive magmas and their respective mantle sources. J. Petrol. 53, 2095–2113.
Keays, R.R., 1995. The role of komatiitic and picritic magmatism and S-saturation in the formation of the ore deposits. Lithos 34, 1–18.
Li, C., Ripley, E.M., 2011. The Jinchuan Ni–Cu–(PGE) deposit: tectonic setting, magma evolution, ore genesis, and exploration implications. Soc. Econ. Geol. Spec. Publ. 17, 164–180.
Li, J., Xu, J.F., Suzuki, K., He, B., Xu, Y.G., Ren, Z.Y., 2010. Os, Nd and Sr isotope and trace element geochemistry of the Muli picrites: insights into the mantle source of the Emeishan Large Igneous Province. Lithos 119, 108–122.
Li, C., Tao, Y., Qi, L., Ripley, E.M., 2012. Controls on PGE fractionation in the Emeishan picrites and basalts: constraints from integrated lithophile–siderophile elements and Sr–Nd isotopes. Geochim. Cosmochim. Acta 90, 12–32.
Liu, J.H., Liu, F.T., He, J.K., Chen, H., You, Q.Y., 2001. Study of seismic tomography in Panxi paleorift area of southwestern China—structural features of crust and mantle and their evolution. Sci. China Earth Sci. 44, 277–288.
Locmelis, M., Pearson, N.J., Barnes, S.J., Fiorentini, M.L., 2011. Ruthenium in komatiitic chromite. Geochim. Cosmochim. Acta 75, 3645–3661.
Ma, Y.X., Ji, X.T., Li, J.C., Huang, M., Kan, Z.Z., 2003. Mineral Resources of the Panzhihua Region. Sichuan Science and Technology Press, Chengdu (275 pp. (in Chinese)).
Ma, Y.S., Tao, Y., Zhong, H., Zhu, F.L., Wang, X.Z., 2009. Geochemical constraints on the petrogenesis of the Abulangdang ultramafic intrusion, Sichuan Province, China. Acta Petrol. Sin. 25, 1146–1158.
McDonough, W.F., Sun, S.-S., 1995. Composition of the Earth. Chem. Geol. 120, 223–253.
Nielsen, R.L., Gallahan, W.E., Newberger, F., 1992. Experimentally determined mineral-melt partition coefficients for Sc, Y and REE for olivine, orthopyroxene, pigeonite, magnetite and ilmenite. Contrib. Mineral. Petrol. 110, 488–499.
Nimis, P., 1995. A clinopyroxene geobarometer for basaltic systems based on crystal-structure modeling. Contrib. Mineral. Petrol. 121, 115–125.
Nimis, P., 1999. Clinopyroxene geobarometry of magmatic rocks. Part 2. Structural geobarometers for basic to acid, tholeiitic and mildly alkaline magmatic systems. Contrib. Mineral. Petrol. 135, 62–74.
Pang, K.-N., Li, C., Zhou, M.-F., Ripley, E.M., 2008a. Abundant Fe–Ti oxide inclusions in olivine from the Panzhihua and Hongge layered intrusions, SW China: evidence for early saturation of Fe–Ti oxides in ferrobasaltic magma. Contrib. Mineral. Petrol. 156, 307–321.
Pang, K.-N., Zhou, M.-F., Lindsley, D., Zhao, D., Malpas, J., 2008b. Origin of Fe–Ti Oxide ores in mafic intrusions: evidence from the Panzhihua Intrusion, SW China. J. Petrol. 49, 295–313.
Pang, K.-N., Li, C., Zhou, M.-F., Ripley, E.M., 2009. Mineral compositional constraints on petrogenesis and oxide ore genesis of the late Permian Panzhihua layered gabbroic intrusion, SW China. Lithos 110, 199–214.
Pearson, D.G., Irvinea, G.J., Ionovb, D.A., Boydc, F.R., Dreibus, G.E., 2004. Re–Os isotope systematics and platinum group element fractionation during mantle melt extraction: a studyof massif and xenolith peridotite suites. Chem. Geol. 208, 29–59.
Qi, L., Wang, C.Y., Zhou, M.-F., 2008. Controls on the PGE distribution of Permian Emeishan alkaline and peralkaline volcanic rocks in Longzhoushan, Sichuan Province, SW China. Lithos 106, 222–236.
Ramsay, W.R.H., Crawford, A.J., Foden, J.D., 1984. Field setting, mineralogy, chemistry, and genesis of arc picrites, New Georgia, Solomon Islands. Contrib. Mineral. Petrol. 88, 386–402.
Roeder, P.L., Emslie, R.F., 1970. Olivine-liquid equilibrium. Contrib. Mineral. Petrol. 29, 275–289.
Rohrbach, A., Schuth, S., Ballhaus, C., Münker, C., Matveev, S., Qopoto, C., 2005. Petrological constraints on the origin of arc picrites, New Georgia Group, Solomon Islands. Contrib. Mineral. Petrol. 149, 685–698.
Rollinson, H.R., 1994. Using geochemical data: evaluation, presentation, interpretation. Longman Scientific & Technical. John Wiley & Sons. Inc., New York pp. 106–117.
Schuth, S., Rohrbach, A., Münker, C., Ballhaus, C., Garbe-Schönberg, D., Qopoto, C., 2004. Geochemical constraints on the petrogenesis of arc picrites and basalt, New Georgia Group, Solomon Islands. Contrib. Mineral. Petrol. 148, 288–304.
Shellnutt, J.G., Iizuka, Y., 2012. Oxidation zonation within the Emeishan large igneous province: evidence from mantle-derived syenitic plutons. J. Asian Earth Sci. 54–55, 31–40.
Shellnutt, J.G., Zhou, M.-F., Zellmer, G.F., 2009. The role of Fe–Ti oxide crystallization in the formation of A-type granitoids with implications for the Daly gap: an example from the Permian Baima igneous complex, SW China. Chem. Geol. 259, 204–217.
Shirey, S.B., Walker, R.J., 1998. The Re–Os isotope system in cosmochemistry and high-temperature geochemistry. Annu. Rev. Earth Planet. Sci. 26, 423–500.
Simkin, T., Smith, J.V., 1970. Minor-element distribution in olivine. J. Geol. 78, 304–325.
Song, X.Y., Zhou, M.-F., Hou, Z.Q., Cao, Z.M., Wang, Y., Li, Y., 2001. Geochemical constraints on the mantle source of the Upper Permian Emeishan continental flood basalts, southwestern China. Int. Geol. Rev. 43, 213–225.
Sun, S.S., McDonough, W.F., 1989. Chemical and isotopic systematics of oceanic basalts: implications for mantle composition and processes. In: Saunders, A.D., Norry, M.J. (Eds.), Magmatism in the ocean basins. Geological Society of Specical Publications, 42, pp. 313–345.
Tao, Y., Li, C., Song, X.Y., Ripley, E.M., 2008. Mineralogical, petrological, and geochemical studies of the Limahe mafic–ultramatic intrusion and associated Ni–Cu sulfide ores, SW China. Mineral. Deposita 43, 849–872.
Tappe, S., Foley, S.F., Stracke, A., Romer, R.L., Kjarsgaard, B.A., Heaman, L.M., Joyce, N., 2007. Craton reactivation on the Labrador Sea margins: $^{40}Ar/^{39}Ar$ age and Sr–Nd–Hf–Pb isotope constraints from alkaline and carbonatite intrusives. Earth Planet. Sci. Lett. 256, 433–454.
Tuff, J., Takahashi, E., Gibson, S.A., 2005. Experimental constraints on the role of garnet pyroxenite in the genesis of high-Fe mantle plume derived melts. J. Petrol. 46, 2023–2058.
Walker, D.A., Cameron, W.E., 1983. Boninite primary magmas: evidence from Cape Vogel Peninsula, PNG. Contrib. Mineral. Petrol. 83, 150–158.
Walker, R.J., Morgan, J.W., Horan, M.F., Czamanske, G.K., Krogstad, E.J., Likhachev, A.P., Kunilov, V.A., 1994. Re–Os isotope evidence for an enriched-mantle plume source for the Noril'sk-type ore-bearing intrusions, Siberia. Geochim. Cosmochim. Acta 58, 4179–4198.
Walker, R.J., Storey, M., Kerr, A.C., Tarney, J., Arndt, N.T., 1999. Implications of ^{187}Os isotopic heterogeneities in a mantle plume: evidence from Gorgona Island and Curacao. Geochim. Cosmochim. Acta 63, 713–728.
Wang, F.G., 1990. Geological characteristics for a dunite body from Sichuan–Yunnan area. Miner. Rocks 39, 61–69 (in Chinese with English abstract).
Wang, C.Y., Zhou, M.-F., 2013. New textural and mineralogical constraints on the origin of the Hongge Fe–Ti–V oxide deposit, SW China. Mineral. Deposita 48, 787–798.
Wang, C.Y., Zhou, M.-F., Zhao, D.G., 2005. Mineral chemistry of chromite from the Permian Jinbaoshan Pt–Pd-sulphide-bearing ultramafic intrusion in SW China with petrogenetic implications. Lithos 83, 47–66.
Wang, C.Y., Zhou, M.-F., Qi, L., 2007. Permian flood basalts and mafic intrusions in the Jinping (SW China)–Song Da (northern Vietnam) district: mantle sources, crustal contamination and sulfide segregation. Chem. Geol. 243, 317–343.
Wang, C.Y., Zhou, M.-F., Zhao, D.G., 2008. Fe–Ti–Cr oxides from the Permian Xinjie mafic–ultramafic layered intrusion in the Emeishan large igneous province, SW China: crystallization from Fe- and Ti-rich basaltic magmas. Lithos 102, 198–217.
Wang, C.Y., Zhou, M.-F., Qi, L., 2011. Chalcophile element geochemistry and petrogenesis of high-Ti and low-Ti magmas in the Permian Emeishan large igneous province, SW China. Contrib. Mineral. Petrol. 161, 237–254.
Wang, C.Y., Zhou, M.-F., Sun, Y.L., Arndt, N.T., 2012. Differentiation, crustal contamination and emplacement of magmas in the formation of the Nantianwan mafic intrusion of the ~260 Ma Emeishan large igneous province, SW China. Contrib. Mineral. Petrol. 164, 281–301.
Weaver, B.L., Tarney, J., 1984. Empirical approach to estimating the composition of the continental crust. Nature 310, 575–577.
Whitaker, M.L., Nekvasil, H., Lindsley, D.H., Difrancesco, N.J., 2007. The role of pressure in producing compositional diversity in intraplate basaltic magmas. J. Petrol. 48, 365–393.
Wilson, M., 1989. Igneous Petrogenesis. Unwin Hyman, London pp. 10–100.
Xiao, L., Xu, Y.G., Mei, H.J., Zheng, Y.F., He, B., Pirajno, F., 2004. Distinct mantle sources of low-Ti and high-Ti basalts from the western Emeishan large igneous province, SW China: implications for plume–lithosphere interaction. Earth Planet. Sci. Lett. 228, 525–546.
Xu, Y.G., Chung, S.-L., Jahn, B.-M., Wu, G.Y., 2001. Petrologic and geochemical constraints on the petrogenesis of Permian–Triassic Emeishan flood basalts in southwestern China. Lithos 58, 145–168.
Xu, Y.G., He, B., Chung, S.-L., Menzies, M.A., Frey, F.A., 2004. Geologic, geochemical, and geophysical consequences of plume involvement in the Emeishan flood-basalt province. Geology 32, 917–920.
Xu, J.F., Suzuki, K., Xu, Y.G., Mei, H.J., Li, J., 2007. Os, Pb, and Nd isotope geochemistry of the Permian Emeishan continental flood basalts: insights into the source of a large igneous province. Geochim. Cosmochim. Acta 71, 2104–2119.
Yan, D.P., Zhou, M.-F., Song, H.L., Wang, X.W., Malpas, J., 2003. Origin and tectonic significance of a Mesozoic multi-layer overthrust system within the Yangtze Block (South China). Tectonophysics 361, 239–254.
Yuan, X.C., 1989. On the deep structure of the Kang-dian rift. Acta Geol. Sin. 63, 1–13 (in Chinese).
Zhang, Y.X., Lou, Y., Yang, X., 1988. The Panxi Rift. Geological Press, Beijing p. 422 (in Chinese).
Zhang, Z.C., Mao, J.W., Mahoney, J.J., Wang, F.S., Qu, W.J., 2005. Platinum group elements in the Emeishan large igneous province, SW China: implications for mantle sources. Geochem. J. 39, 371–382.
Zhang, Z.C., Mahoney, J.J., Mao, J.W., Wang, F.S., 2006. Geochemistry of picritic and associated basalt flows of the Western Emeishan Flood Basalt Province, China. J. Petrol. 47, 1997–2019.

Zhang, Z.C., Zhi, X.C., Chen, L., Saunders, A.D., Reichow, M.K., 2008. Re–Os isotopic compositions of picrites from the Emeishan flood basalt province, China. Earth Planet. Sci. Lett. 276, 30–39.
Zhang, Z.C., Mao, J.W., Saunders, A.D., Ai, Y., Li, Y., Zhao, L., 2009. Petrogenetic modeling of three mafic–ultramafic layered intrusions in the Emeishan large igneous province, SW China, based on isotopic and bulk chemical constraints. Lithos 113, 369–392.
Zhong, H., Zhu, W.G., 2006. Geochronology of layered mafic intrusions from the Pan-Xi area in the Emeishan large igneous province, SW China. Mineral. Deposita 41, 599–606.
Zhong, H., Yao, Y., Hu, S.F., Zhou, X.H., Liu, B.G., Sun, M., Zhou, M.-F., Viljoen, M.J., 2003. Trace-element and Sr–Nd isotopic geochemistry of the PGE-bearing Hongge layered intrusion, Southwestern China. Int. Geol. Rev. 45, 371–382.
Zhong, H., Qi, L., Hu, R.Z., Zhou, M.-F., Gou, T.Z., Zhu, W.G., Liu, B.G., Chu, Z.Y., 2011. Rhenium–osmium isotope and platinum–group elements in the Xinjie layered intrusion, SW China: implications for source mantle composition, mantle evolution, PGE fractionation and mineralization. Geochim. Cosmochim. Acta 75, 1621–1641.
Zhou, C.L., 1982. Petrological characteristics and genesis of the Xinjie basic/ultrabasic layered intrusion in Miyi. J. Chengdu Coll. Geol. 2, 5–12 (in Chinese).
Zhou, M.-F., Kerrich, R.W., 1992. Morphology and composition of chromite in komatiites from the Belingwe greenstone belt, Zimbabwe. Can. Mineral. 30, 303–317.
Zhou, M.-F., Malpas, J., Song, X.Y., Kennedy, A.K., Robinson, P.T., Sun, M., Lesher, C.M., Keays, R.R., 2002a. A temporal link between the Emeishan large igneous province (SW China) and the end-Guadalupian mass extinction. Earth Planet. Sci. Lett. 196, 113–122.
Zhou, M.-F., Yan, D.P., Kennedy, A.K., Li, Y., Ding, J., 2002b. SHRIMP U–Pb zircon geochronological and geochemical evidence for Neoproterozoic arc-magmatism along the western margin of the Yangtze Block, South China. Earth Planet. Sci. Lett. 196, 51–67.
Zhou, M.-F., Robinson, P.T., Lesher, C.M., Keays, R.R., Zhang, C.J., Malpas, J., 2005. Geochemistry, petrogenesis, and metallogenesis of the Panzhihua gabbroic layered intrusion and associated Fe–Ti–V-oxide deposits, Sichuan Province, SW China. J. Petrol. 46, 2253–2280.
Zhou, M.-F., Arndt, N.T., Malpas, J., Wang, C.Y., Kennedy, A.K., 2008. Two magma series and associated ore deposit types in the Permian Emeishan large igneous province, SW China. Lithos 103, 352–368.
Zhu, D., Luo, T.Y., Gao, Z.M., Zhu, C.M., 2003. Differentiation of the Emeishan flood basalts at the base and throughout the crust of southwest China. Int. Geol. Rev. 45, 471–477.
Zindler, A., Hart, S.R., 1986. Chemical geodynamics. Annu. Rev. Earth Planet. Sci. 14, 493–571.